Development of a Real Time Trimodal Spectroscopy

Diagnostic Tool for Barrett's Esophagus

by

Austin H Kim

Submitted to the Department of Electrical Engineering and Computer Science

in Partial Fulfillment of the Requirements for the Degrees of

Bachelor of Science in Electrical [Computer] Science and Engineering

and Master of Engineering in Electrical Engineering and Computer Science

at the Massachusetts Institute of Technology

August 22, 2002

[September 2002]

Author _____
Department of Electrical Engineering and Computer Science
August 22, 2002

Certified by _____
Michael S Feld
Thesis Supervisor

Accepted by _____
Arthur C. Smith
Chairman, Department Committee on Graduate Theses

Development of a Real Time Trimodal Spectroscopy
Diagnostic Tool for Barrett's Esophagus
by
Austin H Kim

Submitted to the
Department of Electrical Engineering and Computer Science

August 22, 2002

In Partial Fulfillment of the Requirements for the Degree of
Bachelor of Science in Computer [Electrical] Science and Engineering
and Master of Engineering in Electrical Engineering and Computer Science

ABSTRACT

Barrett's esophagus (BE) is a condition of the lower esophagus caused by gastroesophageal reflux disease. Patients with BE have an increased probability of developing dysplasia, an abnormal growth or development of cells. This dysplasia in BE is a precursor to cancer of the esophagus, but is currently difficult to detect and diagnose. If the dysplasia is allowed to progress to cancer, it is very difficult to treat successfully. Treatment for dysplasia itself, however, is very effective if done at an early stage. The goal of this thesis project will be to develop a real-time tool that uses spectroscopy to improve upon the methods of detecting dysplasia in BE. This will involve analyzing spectra acquired from patients with BE using models and extracting quantitative information on different aspects of tissue morphology and biochemistry. Using this information, diagnostic algorithms will be developed, optimized and displayed to the physician through a useful interface.

Thesis Supervisor: Michael Feld
Title: Director, MIT Spectroscopy Laboratory

i
Contents

ii
acknowledgements

first of all, i would like to thank those at mit who made this thesis possible. to my advisor, professor Michael Feld, thank you for your guidance and patience, especially for putting up with my last minute drafts. thank you to Irene Georgakoudi, my postdoc, who worked tirelessly and pushed me through this whole endeavor and without whom none of this would have happened. i would like to thank Jelena Mirkovic and Sasha McGee, whose work was also a part of this thesis. thank you to Mike Wallace and Christian Jost, who i never really got to meet but who supplied me with the data for this project. and a thank you to James Tunnel who came through at the end to help me with my final revision. thank you also to Anne Hunter, who's the best course administrator ever.

i would also like to thank my family, without whom i would not be alive, let alone have to worry about a thesis. to my mom and dad, what can i say but thank you, for your continuous prayers, support, trust and love, even when things didn't always work out.

thanks to my brothers, Abe and Ben, who were also always there praying for me and encouraging me.

and to my spiritual family, i know and you know i could not have made it without your prayer and support. thank you to Pastor Paul and Becky JDSN, who give me the privilege to live at concord and be discipled under them, for your undeserved prayers and love. thank you Pastor Chris and Sally SMN for being my spiritual parents, and for your prayers and concern even from out in silicon valley. thank you Dave JDSN and Angela SMN, James hyung, and the MIT cell staff—Susie nuna, Donald hyung, Jungyoon nuna, Julie nuna, and Teresa nuna for emails, phone calls, care packages, concrete reminders of the prayer and support that i did not deserve. thanks to the mit undergrad brothers for your prayers and late night fellowship. thank you to Isaac hyung for the unlimited caffeine. and thanks to my concord brothers, Eugene and Orton for your friendship and support, even from japan and even when i didn't write, Matthew hyung and Walter hyung for unhesitating car loans, Danny hyung for your rides and constant concern, Hero hyung for making sure i was eating, Eddie hyung for putting up with my side of the room for the past many months, Patrick for the headphones that you probably haven't seen for a while, JBau for helping me get into m.eng in the first place, David Chung for always cheering me up, and Jinu hyung for literally being there with me for some of the longest nights of my life. i apologize to all for dragging this out so long and causing you much grief. but i'm finally done!!!

and last, but by far the greatest, thank You to my God the Father and His Son Jesus Christ. thank You for the life you give me, for Your grace and mercy that brought me through this trial that allowed me to see a little more clearly my utter need for You.

1
Introduction

Optics and medicine

The advancement of medical technology has allowed today's physician to have an array of techniques to diagnose and treat disease. Imaging techniques, for example, include such different methods as magnetic resonance imaging (MRI), ultrasound, x-ray, and computed tomography (CT), to name just a few. The availability of such a wide variety of options, along with the continual development of new techniques, while undoubtedly aiding doctors, also suggests that each one of these techniques has its limitations. One needs look no further than the examples mentioned to find drawbacks in each: both x-ray and CT use potentially harmful radiation, MRI and ultrasound provide images only at low resolutions and thus are only effective when larger, morphological changes are involved. Yet it is these very techniques that are the basis of the current diagnostic methods used to detect precancerous changes. Early detection is a vital element in the treatment of cancer, as it is in these stages, before the actual development into cancer that treatment is most

effective. Unfortunately, another shortcoming of the four techniques that they all have in common is their inability to diagnose lesions at a microscopic level, the early stage in which the treatment is easily effective.

A potential solution lies in the use of light. Light has been used in the detection and recognition of disease beyond its simple reception into the naked eye since the mid-1800s and the improvement of the microscope. Since then, the exploitation of light has evolved into many different forms. Light is used not only to recognize disease, but also to treat it through such applications as laser ablation, photodynamic therapy, and laser hyperthermia. Laser ablation is the use of lasers to effect mechanical changes in tissue, cutting and shaping it by using short pulses of laser light at high powers to remove irradiated tissue.[1,2] Photodynamic therapy brings about chemical changes in tissue, interacting with molecules found or placed in diseased tissue to produce a chemical reaction.[3] The reaction produced results in cellular necrosis and destruction of the diseased tissue. Laser hyperthermia induces a thermal change in tissue, raising temperatures to burn or even vaporize the targeted tissue.[4] These examples of mechanical, chemical, and thermal changes are but a few of the classifications of the effects light can have on tissue.

Light does not have the disadvantages found in the current cancer imaging methods, as it is not harmful to the body, and the short wavelength of light allows for sub-cellular resolutions of images. In addition, optical techniques and the instruments that use them are generally not as complex as many of the other current imaging instruments, costing less money, requiring less maintenance and generally less specified training. Also, they are typically non-invasive, able to obtain data *in vivo* and present it to a physician in real time to make clinical decisions on the spot. Some of these techniques include reflectance, fluorescence, light scattering, and Raman. Reflectance, fluorescence, and light scattering will be discussed in further detail later in this thesis. Raman spectroscopy involves measuring a shift in the frequency of the light waves created by the vibrations of the molecules in the tissue under examination. These

---

[1] Dixon, et al.
[2] Itzkan, et al.
[3] Dougherty
[4] Anghilery, et al.

vibrations are dependent upon the chemical composition of the tissue, making Raman useful for the measurement of the concentrations of various components found in tissue, such as proteins, glucose, lipids, and nucleic acids. With this concentration information, the state of the tissue can be discerned; for example, Raman spectroscopy has been used to diagnose breast malignancies[5] and atherosclerosis in the coronary artery.[6]

Motivation

Barrett's esophagus is a condition in which the cells lining the lower portion of the esophagus stop looking like normal esophageal cells, and start looking more like the cells that line the colon. About five to ten percent of people with Barrett's esophagus develop cancer,[7] and compared with the rest of the population, people with Barrett's have an estimated forty times greater chance to develop lower esophageal cancer, or *adenocarcinoma*.[8] The incidence in cancers arising in Barrett's esophagus is increasing more rapidly than any other cancer in the United States.[9] Once Barrett's esophagus advances to the stage of adenocarcinoma, it is, as with all cancers, very difficult to treat. Dysplasia in Barrett's esophagus, a precancerous condition, on the other hand, is readily treatable, but current methods of detection are not entirely effective. From these facts, it is clear that a tool to assist doctors in the detection of dysplasia in Barrett's esophagus would prevent the development of cancer and ultimately save lives.

This project furthers the development of a diagnostic tool that can potentially be used to aid physicians in detecting dysplasia in Barrett's esophagus at an early, treatable stage. This is accomplished through tri-modal spectroscopy, a mode of spectroscopy that combines reflectance, fluorescence, and light scattering spectroscopy techniques. A diagnostic algorithm is developed to use this spectroscopic technique in a clinical setting in real-time to ultimately allow this tool to be used as a guide to take better advantage of biopsy and make it a less random selection process. In addition, some of the information

[5] Manoharan, et al.
[6] Brennan, et al.
[7] National Institute of Health
[8] Ridell et al.

obtained through these spectroscopic techniques in diagnosing various stages of precancer have never been analyzed previously, and should provide a basis for further understanding of the biochemical changes involved in the early development of precancerous changes.

[9] Fred Hutchinson Cancer Research Center

2
Background

Epithelial Tissue

Human tissue can be categorized into four types: epithelium, connective tissue, muscle, and nervous tissue. These tissues are made up of variable quantities of cells and extracellular matrix, and these tissues in turn make up the functional units called organs. The esophagus, for example, consists of an epithelial layer on its inner surface covering layers of connective tissue and muscle containing nerves and blood vessels. Blood vessels can be considered a specialized subtype of connective tissue. Organs are then categorized into organ systems, such as skeletal, muscular, circulatory, and in the case of the esophagus, gastrointestinal.

The epithelial tissue is of particular interest because it is only this surface area that is readily accessible by light spectroscopy. However, access to only superficial tissue layers is not problematic, because more than 85% of all cancers occur in the epithelial

layer, and the detection of precancerous changes in this layer is still considered one of the greatest challenges of modern medicine.[10]

Epithelial tissue is classified in different ways. Based on the number of cell layers, it is divided into simple, stratified, pseudostratified, and transitional. Normal esophageal epithelium is stratified, meaning it is formed by a number of cell layers, but the epithelium of Barrett's mucosa is simple. The epithelial tissue is also classified according to the shape of the cells that compose the tissue. These classifications are squamous, cuboidal, and columnar. The epithelium of the esophagus is squamous, or flat-shape celled, stratified epithelium, a common subtype of stratified epithelium. This subtype is made up of cells that flatten out while they move from the inner layer to the surface layer as the cell matures. The epithelial tissue of the stomach and colon, on the other hand, is columnar epithelial tissue, or composed of a single layer of cells that are cylindrically shaped.

Barrett's esophagus

The esophagus is a muscular tube that connects the mouth to the stomach and provides the channel of transportation of food. The esophagus is separated from the stomach by a strong muscular valve called the *lower esophageal sphincter* (LES). This valve usually remains shut and opens only to allow food to pass from the esophagus to the stomach. However, if the LES is not functioning properly, the acid found in the stomach that is used to help digest food can reflux back into the esophagus. This is what causes the pain of heartburn and indigestion. If this continues to occur over a period of time, it can lead to an inflammation of the esophagus (*esophagitis*) or *gastroesophageal reflux disease* (GERD), a condition that affects about 20% of the adult population in the United States.[11] From there, about 12.5% of people with GERD go on to develop Barrett's esophagus.[12,13]

---

[10] Cotran, et al.
[11] Gopal
[12] Winters, et al.
[13] Schnell, et al.

The squamous cells of the esophagus and the columnar cells of the stomach and colon are distinctly different in appearance and architecture, and normally there is a clear border between the end of the esophagus and the opening of the stomach. These cells are different as they serve different functions; the cells of the stomach need to be resistant to the acid to which it is constantly exposed, while the squamous cells need no such protection. If, however, the esophagus begins to be exposed to stomach acid, as is the case with GERD, the squamous cells can be replaced by columnar cells, possibly as a defense mechanism to prevent further damage to the esophagus. This is called *metaplasia*, the finding of cells of another type not normally found in an organ. In the case of Barrett's esophagus, mucin-producing cells typically found in the colon are found comprising specialized columnar epithelium in the esophagus. This layer of columnar cells is a single-cell layer, as opposed to the several layers of squamous cells that normally make up the esophageal epithelium. With the reduction in thickness, the underlying blood vessels become more visible, making the metaplastic tissue look more reddish in appearance (figure 2.1).

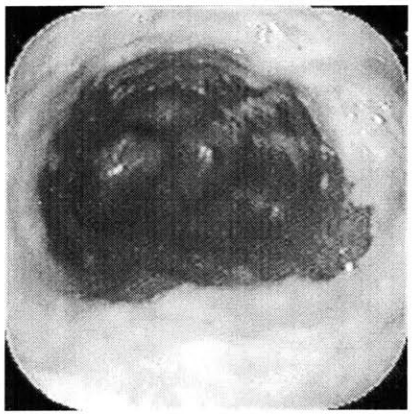

Figure 2.1

In ten to twenty percent of Barrett's patients, the specialized columnar cells exhibit *dysplasia*. Dysplasia is a precancerous condition with the abnormal growth or development of cells, histological changes that are present only in the epithelial layer and not in the stroma. This can be an alteration in size, shape, and/or organization of cells. The variation in size and shape of the cells and nuclei is called *pleomorphism*. The cell nuclei can also become *hyperchromatic*, or appear darker when stained with nuclear dyes because of excessive amounts of chromatin. Enlarged cell nuclei and nuclear crowding are also typical signs of dysplasia. The higher-level organization of the epithelium can also be disrupted, closely related to the loss of normal maturation of cells. Dysplastic epithelia progress from low-grade to high-grade dysplasia, diagnosed by the severity and spread of the deformations in the cells.

From high-grade dysplasia, the condition worsens to lower esophageal cancer, which is an adenocarcinoma. As aforementioned, it is difficult to detect these cancers until they are too advanced to be cured. The condition of dysplasia almost always precedes that of the development of cancer. Though it does not necessarily result in cancer, dysplastic cells can be said to have malignant potential. As a result, dysplastic surveillance is considered a crucial step in cancer prevention, since dysplasias, if detected, can usually be cured with surgery or other therapies.

Unfortunately, this detection is quite difficult in practice. Currently, esophageal dysplasia is detected through endoscopy and biopsy. Endoscopy involves using a long thin tube guided through the mouth to look at and examine the tissue of the esophagus. The endoscope also has accessory channels that allow the doctor to insert instruments to perform the biopsy, or in other words, remove small samples of tissue that are analyzed in a laboratory by a histopathologist. The pathologist takes the removed tissue sample and places it in a fixative, which cross-links, or fixes the proteins in the cells. This fixed sample is then embedded in paraffin wax, cut into thin slices, and then stained with a mixture of dyes that facilitate distinguishing different parts of cells. These slices are placed in a glass microscope slide and examined under a microscope. The problem with this procedure is that dysplasia is not visible to the eye during endoscopy, and the dysplastic lesion can range in size, sometimes found to be as small as one millimeter in diameter. The current recommended guideline is to obtain random four-quadrant biopsies (where the esophagus is divided into four quadrants and a sample is taken from each) at two-centimeter intervals,[14] but the probability of detecting a small lesion over the length of two centimeters is not favorable. Moreover, the discipline of pathology is known to be one of part science and part art. Analyzing biopsies is partially qualitative and subjective. Studies have shown that the agreement in diagnoses between pathologists and even between multiple analyses of the same pathologist have in some cases been less than fifty percent.[15,16] In addition, biopsies have the inherent delay in taking samples to a laboratory, analyzing, and then returning with a diagnosis. If further biopsy samples are desired, this is not discovered until the pathologist is at the lab. This difficulty is

[14] Gopal
[15] Reid et al.
[16] Cotran et al.

supported in practice by a Mayo clinic study that suggests that the majority of cases of dysplasia in Barrett's esophagus in the general population are never detected.[17] It is clear that a superior method of diagnosis is necessary.

Spectroscopy

Preliminary studies have assessed the potential of spectroscopy as a tool to diagnose dysplasia in Barrett's esophagus. Spectroscopy is a study of the way light interacts with matter. When light strikes matter, several things can happen. It can be reflected, transmitted, or absorbed. By detecting and measuring the amounts of light that undergo these and other effects, and taking into account the conservation of energy and matter, the full interaction of the light with the object can be understood. The different reactions of light with matter can be used in a number of ways to understand various factors about the object under study.

Specifically, spectroscopy can be used to observe and analyze tissues at the cellular and sub-cellular levels. There are many current techniques that make use of the different ways in which light interacts with cells to provide structural and functional information about tissue. Since dysplastic tissue is fundamentally different from healthy tissue in structural and functional ways that are not easily macroscopically differentiated, spectroscopy can be an effective method for detecting dysplasia. Furthermore, the advantages of optical diagnostic techniques do apply specifically to spectroscopy. It works well in diagnosis as it is non-invasive and it can be applied within the body by using optical fibers that are compatible with an endoscope. Physicians are already familiar with the use of an endoscope, so little or no special training is needed. Since it can be applied within the body without any need for tissue removal, unlike the case with biopsies, information can be conveniently gathered from many different sites with the results returned in real time. Finally, it also allows for a more objective analysis, as the returned results are quantitative measurements, as opposed to the potentially subjective histological analysis of biopsies. As these quantitative measurements are direct

[17] Cameron et al.

reflections of what is happening in the tissue, the information revealed by these measurements about tissue morphology and biochemistry will also lead to a better understanding of the process undergone by tissue in the development of cancer.

Diffuse reflectance spectroscopy

Reflectance spectroscopy is one of the simplest techniques for studying biological tissue, and has been used by several researchers,[18,19] including specifically the detection of precancerous and cancerous transformations in the esophagus.[20] It has been used to differentiate between dysplastic and non-dysplastic tissue in the cervix[21] and oral cavity,[22] and also diagnostically in tissues such as colon,[23,24] bladder,[25] and breast,[26] to name a few. The typical instrumentation setup for reflectance spectroscopy involves an optical fiber probe that is used to deliver white light from a high-power lamp onto the tissue and to collect the diffuse reflectance. These probes are often incorporated into endoscopes or catheters, allowing easy, non-invasive access to tissue of several organs including the esophagus. This probe is used to deliver light to the tissue surface, which then undergoes multiple scattering and absorption. Part of the light returns as diffuse reflectance, and this light carries the quantitative information about the tissue's scattering and absorption properties. Light scattering in tissue is considered one of the main difficulties in biomedical spectroscopy, as it randomizes the path of the photons in the tissue, making difficult the calculation of its origin and trajectory. Reflectance spectroscopy, instead of trying to eliminate this scattering component, uses it to gain insight into the tissue morphology and organization, as different cellular structures have distinct scattering patterns. The scattering is caused by disparities in the refractive index of structures found in tissue like collagen fibrils, cell membranes, cell nuclei, and

[18] Liu et al.
[19] Zonios et al.
[20] Lovat et al.
[21] Georgakoudi et al. (2001)
[22] Muller et al.
[23] Ge et al.
[24] Zonios et al.
[25] Mourant et al. (1995)

mitochondria. For diffuse reflectance in the esophagus, it seems the majority of the scattering can be attributed to collagen fibers,[27] but the exact contributions of each of these scatterers and perhaps others is still not well understood and under investigation.[28,29] By modeling both healthy and diseased tissue, one can differentiate between the scattering patterns of the two.

The absorption properties depend on the concentration of components in the tissue that absorb light at specific wavelengths. A major contributor to the overall tissue absorption in the visible wavelength range is hemoglobin, which exists in a deoxygenated and an oxygenated form, each one of which has distinct absorption features (figure 2.2).[30]

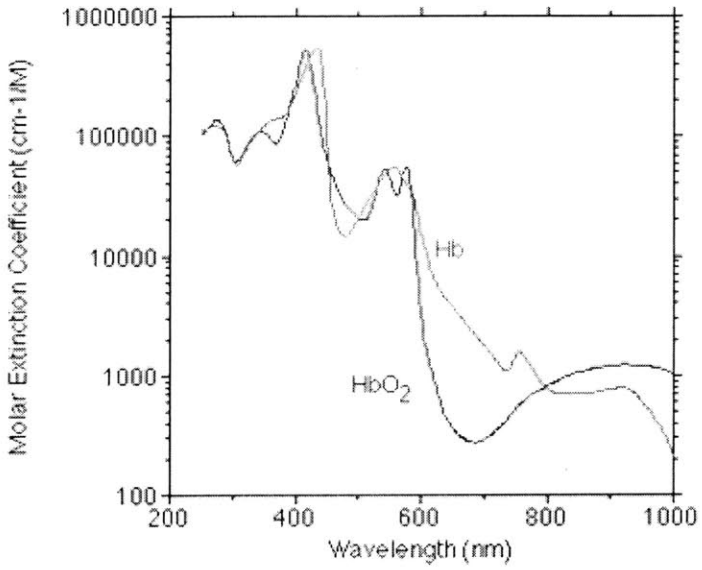

Figure 2.2

Therefore the information collected through diffuse reflectance provides information about the hemoglobin concentration, or how much blood is in the tissue and its oxygenation. Other absorbers include beta-carotene, found noticeably in fatty tissues such as arteries and breast, and melanin, found in tissues such as skin. For the esophagus, however, the dominant absorber is hemoglobin. Both pieces of information, scattering and absorption, can be used in combination to determine whether or not the tissue is dysplastic, as dysplastic tissue properties include those of altered tissue morphology and biochemistry.

A variety of models, statistical, empirical, and theoretical, have been developed using the spectra returned by diffuse reflectance spectroscopy. One empirical algorithm,

---

[26] Bigio et al. (2000)
[27] Saidi et al.
[28] Leonard et al.
[29] Mourant et al.

for example, computes the area under the normalized reflectance curve between 540 and 580 nm and the area under the curve from 400 to 420 nm and takes this ratio to differentiate neoplastic from non-neoplastic colon tissues.[31] Another takes the slope of the reflectance in the 330 to 370 nm range to tell apart malignant from non-malignant bladder tissues.[32] Statistical algorithms based on neural network pattern recognition have been developed to distinguish neoplastic features in skin,[33] breast,[34] and colon.[35] A more rigorous theoretical model was also developed describing the tissue reflectance as a function of absorption and reduced scattering coefficients. This is the model developed by Zonios, and will be discussed more in depth in chapter four, as it is the model that was employed in this study.

Fluorescence spectroscopy

In fluorescence spectroscopy, the tissue is excited using a laser or filtered lamp illumination at certain wavelengths. This excitation is applied similar to diffuse reflectance spectroscopy, with fiber optics again providing a convenient method to access tissue. The tissue molecules absorb the energy, become excited, and fluoresce when the absorbed energy is re-emitted as the molecule returns to its ground state. The fluorescence is affected by the chemical and architectural composition of the tissue, namely the presence of tissue fluorophores such as collagen, tryptophan, elastin, reduced nicotinamide adenine dinucleotide (NADH), flavin adenine dinucleotide (FAD), and porphyrins. As the tissue undergoes changes in pH, metabolic state, and architecture, the fluorescence spectra measured change in shape and intensity.[36,37] Fluorescence spectroscopy has had extensive previous use in detection of such conditions as dyplasia

---

[30] Prahl
[31] Mourant et al. (1996)
[32] Mourant et al. (1995)
[33] Wallace et al.
[34] Bigio et al. (2000)
[35] Ge et al.
[36] Bigio et al. (1997)
[37] Zonios et al.

in the bladder,[38] atherosclerosis of the aorta and coronary artery,[39] brain stroke,[40] and also cancer[41] and dysplasia in the esophagus.[42]

The fluorescence measurements can be affected by the scattering and absorption from the tissue particles around it, as tissue is a turbid medium. As aforementioned, these same distortions that are useful in reflectance spectroscopy, make meaningful interpretation of the spectra in fluorescence spectroscopy very difficult. If gross enough, the distortions can mask completely any biochemical changes that the tissue undergoes from non-dysplastic to dysplastic. Only by removing these distortions can the spectra be interpreted and the biochemical changes be quantitatively measured.

It has been observed that fluorescence photons and reflectance photons undergo similar distortions by scattering and absorption. As a result, diffuse reflectance spectra can be used to remove these scattering and absorption distortions from measured fluorescence spectra to extract the intrinsic fluorescence. This technique has been implemented in NAD(P)H monitoring studies in the brain, heart, and liver, and a host of other experiments.[43] The models developed through these previous works involve both linear and non-linear combinations of fluorescence and reflectance spectral features at specific wavelengths, and are discussed in detail in chapter four.

Once the intrinsic fluorescence spectrum is extracted, it can be decomposed into linear combinations of the chromophore fluorescence spectra to determine concentrations of the chromophores found in the tissue. In Barrett's esophagus and also in uterine cervical tissue sites, for example, it was found NADH fluorescence levels increased and collagen fluorescence decreased as tissues progressed from healthy to dysplastic.[44,45] Dysplasia found in the oral cavity has also displayed similar differences in NADH and collagen intensities.[46] In the coronary artery, there are four chromophores identified,

---

[38] Arendt et al.
[39] Richards-Kortum et al.
[40] Schantz et al.
[41] Vo-Dinh et al.
[42] Georgakoudi et al. (2001)
[43] Ince et al.
[44] Georgakoudi et al. (2001)
[45] Georgakoudi et al. (2002)
[46] Muller

three of which may be as useful for diagnosis. As atherosclerosis develops in arteries, collagen,[47] tryptophan,[48] and ceroid[49] are found to increase.

In addition to these endogenous chromophores, or chromophores naturally found in the tissue, exogenous chromophores can also be used to detect disease. Exogenous chormophores are substances which are administered either topically or intravenously, have identifiable fluorescence spectra, and are designed to react differently once introduced to healthy and diseased tissue. Hematoporphyrin derivative, for example, is an exogenous chormophore of interest that accumulates preferentially in tumor tissue.[50] Others that have been used to detect tumors are polyhematoporphyrin,[51] sulphonated phthalocyanines,[52] and benzoporphyrin derivative monoacid.[53]

The models used for fluorescence spectroscopy are generally statistically or empirically drawn algorithms to assess the sensitivity and specificity with which abnormalities can be differentiated from normal tissue. Empirical algorithms usually involve an intensity value or ratio of values at specific excitation-emission wavelengths or wavelength ranges.[54] Most fluorescence imaging diagnostic systems found in clinical settings use some derivation of this approach.[55,56]

Statistically, a very useful tool is principal component analysis.[57] This is the method used to decompose the tissue fluorescence spectra into principal component spectra. Each principal component spectrum is weighted appropriately in a linear combination to best fit the data. These weight values are typically used to determine the spectral features that are different between normal and diseased tissues and to develop corresponding algorithms. Such a technique was used in cervical examination to detect squamous intraepithelial lesions (SILs), and was able to obtain a sensitivity of 82% and a specificity of 68%,[58] where sensitivity is calculated by the number of positives that are

---

[47] Tammi et al.
[48] Laifer et al.
[49] Hoff et al.
[50] Richards-Kortum et al. (1996)
[51] Andersson-Engels et al. (1989)
[52] Andersson-Engels et al. (1993)
[53] Van Leengoed et al.
[54] Panjehpour, et al.
[55] Lam,et al.
[56] Goujon, et al.
[57] Jackson JE
[58] Ramanujam et al.

correctly diagnosed out of the total positives, and specificity is the number of negatives that are correctly diagnosed out of the total number of negatives.

As mentioned, measured fluorescence can be distorted by scattering and absorption. A number of models have been developed to remove these distortions, and thus to extract the intrinsic fluorescence. An empirical model developed by Richards-Kortum et al,[59] who expressed measured fluorescence as a combination of two factors. The first is a linear combination of all the fluorophore contributions, the intrinsic fluorescence, and the second is two attenuation factors representing the attenuation due to scattering and to blood absorption. This model has been used quite effectively in fluorescence of arterial tissue excited at 476 nm. It was able to extract fluorescence contributions from structural proteins (collagen and elastin) and ceroid, and the attenuation factors due to hemoglobin (absorption) and structural proteins (scattering).[60] The diagnostic algorithm developed from this study distinguished diseased from normal tissue with a sensitivity of 91% and specificity of 85%.

Light scattering spectroscopy

Light scattering has been used to study a wide variety of materials, from single atoms to complex condensed matter systems.[61] Tissue can be seen as another example of a complex system. The idea behind LSS is similar to DRS, except DRS looks at the photons that undergo multiple scatterings, while LSS measures only those photons that are singly backscattered. LSS is primarily useful for determining the different sizes of sub-cellular particles found in the tissue. For particles with large diameters compared to the wavelength, the scattering is highly peaked in the forward and backward directions, making the nucleus of the cell a major scattering center for light scattered in almost exactly the backward direction. Since the most prominent abnormality found in dysplastic cells is the enlargement and crowding of cell nuclei and organelles within it, this analysis is yet another useful technique in detecting the dysplasia of Barrett's

[59] Richards-Kortum et al. (1989)
[60] Richards-Kortum et al. (1989)
[61] Newton

esophagus before it progresses beyond what can be cured. As biopsy is the current standard in diagnosis of precancerous conditions, this quantitative and more objective perspective to biopsy can be invaluable to the improvement of the current diagnostic standards.

The application of this theory, however, is not trivial. Tissue is a turbid medium, and light entering it is far more prone to multiple scattering than to single scattering. The signal retrieved, therefore, has a much stronger multiple scattering component. Two different solutions to this problem are to physically remove multiply scattered photons, and to theoretically model the diffuse component.

The physical approach would be to use polarized light, as singly back-scattered light retains polarization, while multiple scattered light becomes depolarized.[62] In the theoretical approach, the LSS spectrum is extracted from the measured reflectance spectrum, by modeling and subtracting the diffuse background. By subtracting the diffuse component according to a model developed by Zonios,[63] the LSS spectrum is what is left remaining. This spectrum provides insight into cell nuclear size through the frequency of its intensity oscillations as a function of wavenumber, and the density of scatterers, or the nuclear crowding, through the depth of these variations. These insights are drawn based on the theory of light scattering,[64] As LSS is a newer procedure than that of reflectance and fluorescence spectroscopy, it does not have as extensive a background of clinical results. Nevertheless, LSS has been examined in preliminary studies in precancer detection in Barrett's esophagus,[65] the bladder, the oral cavity, colon,[66] and the uterine cervix[67] with promising results.

---

[62] Sokolov et al.
[63] Zonios et al.
[64] Zonios et al.
[65] Georgakoudi et al. (2001)
[66] Backman
[67] Georgakoudi et al. (2002)

Tri-Modal Spectroscopy

As each of the techniques depends upon different aspects of change in the tissue as it goes from healthy to dysplastic, the combination of these three techniques, called tri-model spectroscopy, has been shown to classify the tissue state with high accuracy in preliminary studies. Previous work done combining these three techniques for the detection of dysplasia in Barrett's esophagus has shown that the tri-modal diagnoses were more consistent with pathology than any of the techniques used individually.[68]

[68] Georgakoudi et al. (2001)

3
Experimental methods

Hardware

The instrument used in this study for data collection is a fast emission-excitation matrix, or FastEEM, apparatus developed at the Spectroscopy Laboratory, which collects both florescence spectra and reflectance spectra. It consists of a 308-nanometer (nm) XeCl excimer laser that pumps a rotating wheel of ten dyes, producing eleven different excitation wavelengths between 308 and 510 nm. There is also a white light source, a Xe flash lamp, used for the reflectance. The white and laser excitation light are coupled to a fiber that delivers light onto the tissue. It is surrounded by six collection fibers that gather the emitted florescence and reflectance light. The collection fibers feed the collected light through a spectrograph to a CCD, which converts the information into data that can be transferred to a computer for analysis. The data for all three types of spectroscopy were collected through this apparatus in less than one second. It is called an

excitation-emission matrix because a series of fluorescence emission spectra are collected at several excitation wavelengths.

The XeCl laser used is an excimer laser, a compound of the words excited dimer, or diatomic molecules. This laser produces a beam 7.5 mm by 4.5 mm, with pulse energies as high as 14 mJ, duration of 15 ns, and rates as high as 200 Hz. It emits at 308 nm, which is lower than the nitrogen laser used in the previous version of the FastEEM. This is valuable, as it allows for the excitation of an additional fluorophore, tryptophan. Although this excitation wavelength can be potentially harmful to human tissue at high intensities, the power used for tissue fluorescence is very weak and does not approach these dangerous levels.

This laser is used to excite the tissue at ten other wavelengths by using a wheel of dyes and filters. Each dye is in its own small container at the edge of a rotating wheel powered by a motor at approximately 0.2 seconds per cycle. As each dye cell falls into position between two mirrors, a trigger signal is generated that fires the laser, and the laser beam is focused at the edge of the dye cell. Dye fluorescence is emitted and amplified as it bounces between the two mirrors. The resulting beam from each dye is focused using another combination of lenses into the optical fiber that delivers the light to the tissue.

This fiber optic probe carries light from both light sources, the laser and the flash lamp. It also consists of the six collection fibers, each three meters long and surrounding the central excitation fiber at the distal tip. The seven fibers are fused together at the tip, serving dual purposes of keeping the fibers together and creating an optical shield. The shield is beveled at an angle of seventeen degrees and polished to minimize the internal reflections when the light passes from the glass tip to the tissue surface. It also provides a fixed delivery and collection geometry, allowing for quantitative study. This probe tip is brought into contact with the tissue sample being measured. Each set of measurements takes about 0.2 seconds to acquire, allowing minimal time for the physician or patient to move.

To further improve data accuracy, a standard calibration procedure is performed before taking measurements. A mercury lamp is used to calibrate the wavelength scale of the spectrograph. A spectralon disk with approximately 20% reflectance over the entire

visible spectral region is used for white light reflectance calibration, to offset the xenon lamp's inherent line shape and intensity. A standard rhodamine B in ethylene glycol solution calibrates for fluorescence intensity, which then allows data sets to be compared despite small system alignment variations. This rhodamine fluorescence response also allows for calibration of the FastEEM system to the varying laser power used at each excitation wavelength, by comparing its response to that of a well-calibrated spectrofluorimeter. Finally, to correct for dark counts of the CCD and fluorescence and reflectance background created by the fiber itself, a background spectrum is taken in open air and subtracted from the data.

Software

The software written for this instrument controls the system, from acquisition to processing of the data. The front end is a Labview-driven graphical user interface that allows the user to see the various spectra, and to compare current data with previously obtained sets. Labview also allows simple data processing such as normalization, and provides a method to interface with the back end data processing procedures through externally called dynamic link library routines. The back end is written in C++ and incorporates the mathematical manipulations the spectral data needed to undergo to be analyzed using quantitative theoretical models and classified using the extracted parameters.

The entire time required for computation, from data acquisition to display with this software is, of course variable dependent on processor speed. Nevertheless, the time is on the order of seconds, entirely reasonable for real time analysis and use in clinical environments to guide physicians as they perform endoscopies to better select biopsy sites.

4
Analysis models

Two types of spectra were collected: fluorescence and reflectance. Using models, the data is analyzed to acquire three types of information based on diffuse reflectance, intrinsic fluorescence, and light scattering spectroscopy. Finally, information from all three techniques is combined in a modality called tri-modal spectroscopy.

Diffuse reflectance model

Initial data analysis steps involve the measured reflectance spectra, which are fit to a mathematical model based on diffusion theory, in which the reflected light is described as a function of the absorption and reduced scattering coefficients of the tissue. Consequently, approximations must be made with appropriate assumptions to make the

scattering problem an approachable one. The model used in this study,[69] one based on diffusion theory, characterizes the scattering behavior as a reduced scattering coefficient, μ_s', defined as

$$\mu_s' = \mu_s (1 - g), \qquad /4.1/$$

where μ_s is the scattering coefficient (unreduced), and g is the anisotropy coefficient, or a parameter describing how much of the scattering is forward directed. The scattering coefficient is defined as

$$\mu_s = \sigma_s \rho, \qquad /4.2/$$

where ρ is the density of scattering particles and σ_s is the scattering cross section. Mie theory is a standard way of estimating σ_s numerically. The anisotropy coefficient is

$$g = 2\pi \int_0^{\pi} p(\theta) \cos\theta \sin\theta d\theta . \qquad /4.3/$$

where $p(\theta)$ is the phase function. One approximation for this phase function is

$$p(\theta) = \frac{1}{4\pi} \frac{1 - g^2}{\left(1 - g^2 + 2g\cos\theta\right)^{3/2}}, \qquad /4.4/$$

but g is also numerically estimated using Mie theory, as none of the phase function approximations have the correct physical properties characterized by Mie theory.

The reduced scattering coefficient parameter essentially simplifies calculations and allows the intensity of multiple scattered, diffusely randomized light to be characterized by two parameters, the reduced scattering coefficient and the absorption coefficient, μ_a. The absorption coefficient is a counterpart to the scattering coefficient, and its definition is similar:

---

[69] Zonios et al.

$$\mu_a = \sigma_a \rho, \qquad /4.5/$$

the absorption cross section multiplied by the molecule density. It can be calculated as a function of hemoglobin concentration by

$$\mu_a(\lambda) = 2.3c\left(a\varepsilon_{HbO_2}(\lambda) + (1-a)\varepsilon_{Hb}(\lambda)\right), \qquad /4.6/$$

where c is the total hemoglobin concentration, a is the oxygen saturation parameter, or the oxy-hemoglobin concentration divided by the total hemoglobin concentration, and ε is the extinction coefficient, which describes the attenuation of radiation traversing the subscripted medium.

The model used in this study was developed by Zonios et al,[70] derived from a model based on the diffusion approximation to the light transport equation.[71] Specifically, this model was simplified to account for the light delivery/collection geometry of the optical fiber probe used in the measurements and it resulted in an analytical expression for the collected reflectance spectrum, which is described by the following expression:

$$R_p(r) = \frac{1}{2}\frac{\mu_s'}{\mu_s' + \mu_a}\left[e^{-\mu \cdot z_0} + e^{-\left(1+\frac{4}{3}A\right)\mu \cdot z_0} - z_0\frac{e^{-\mu \cdot r_1}}{r_1} - \left(1+\frac{4}{3}A\right)z_0\frac{e^{-\mu \cdot r_2}}{r_2}\right], \qquad /4.7/$$

where

$$r_1 = \left[z_0^2 + r_c^2\right]^{1/2},\ r_2 = \left[\left(z_0 + z_0\frac{4}{3}A\right)^2 + r_c^2\right]^{1/2},\ z_0 = \frac{1}{\mu_s' + \mu_a},\ \text{and}\ \mu = \sqrt{3\mu_a\left(\mu_s' + \mu_a\right)}.$$

[70] Zonios et al.
[71] Farrell et al.

Intrinsic fluorescence model

In order to extract intrinsic fluorescence, a rigorous, analytical model was developed based on a photon migration picture from Monte Carlo simulations.[72] This model holds for fluorescence and reflectance measurements acquired over the same wavelength range using identical light delivery and collection geometries. This model was then further improved to be applicable in ranges of significant absorption.[73] This model relates intrinsic fluorescence, f_{xm}, measured fluorescence, F_{xm}, and reflectance, R_m, according to the following equation:

$$f_{xm} = \frac{F_{xm}}{\frac{1}{\mu_{sx}\ell}\sqrt{\frac{R_{0x}R_{0m}}{\varepsilon_x\varepsilon_m}}\frac{R_x}{R_{0x}}\left(\frac{R_m}{R_{0m}}+\varepsilon_m\right)}} . \qquad /4.7/$$

R_o is the reflectance in the case of no absorption, subscripts x and m refer to excitation and emission wavelength, l is a constant dependent on the probe geometry, and ε is also approximately a constant, dependent on the probe geometry and the tissue anisotropy coefficient. This model holds as long as the fluorescence and reflectance are measured with the same probe at the same instant of time, and has been validated using physical tissue models with known optical properties and through clinical studies extracting intrinsic fluorescence from Barrett's esophagus,[74] the uterine cervix,[75] and the oral cavity.[76]

The basis spectra for decomposition of the extracted intrinsic fluorescence also needed to be modeled, as obtaining the spectral features through fluorescence of commercially available versions of the chromophores would not take into account the local environment of the chromophore in the tissue. Instead spectra acquired during progressive deoxygenation of esophageal tissue were decomposed using a multivariate

[72] Wu et al.
[73] Zhang et al.
[74] Georgakoudi et al. (2001)
[75] Georgakoudi et al. (2002b)

curve resolution algorithm, and the resultant components were consistent with collagen and NADH.[77] The multivariate curve resolution technique was employed also to obtain component spectra at the 308 nm excitation wavelength for tryptophan, and at the 400 and 412 nm excitation wavelengths for porphyrin fluorescence spectra, detailed in a later section.

Light scattering model

The LSS analysis uses the same spectrum as used by the DRS. As discussed, LSS involves singly backscattered photons as opposed to DRS, which analyzes multiply scattered photons. The measured reflectance spectrum contains both of these data. The spectrum used for LSS is therefore extracted by taking the reflectance spectrum and subtracting from it the spectrum of multiply scattered photons, leaving behind a singly backscattered photon spectrum. This is then analyzed using an approximation for the scattering cross section developed by van de Hulst,[78] which applies for scattering by particles larger than or comparable to the wavelength of light. His approximation is dependent on the phase shift of the ray as it enters and exits the particle, which in turn depends on the particle shape and refractive index. It is obtained as

$$\sigma_s(\lambda,r)=\frac{1}{2}\pi l^2\left(1-\frac{\sin(2\delta/\lambda)}{\delta/\lambda}+\left(\frac{\sin(\delta/\lambda)}{\delta/\lambda}\right)^2\right), \qquad /4.8/$$

where $\delta = 2\pi r(n\text{-}l)$, $l = 2r$, and n the relative refractive index, or the ratio of the scattering particle's refractive index to the index of its immediate surroundings.

Previous work using LSS on Barrett's esophagus analyzed the degree of nuclear crowding, looking at the number of nuclei per square millimeter, and the percentage of

[76] Muller et al.
[77] Georgakoudi et al. (2002a)
[78] Van de Hulst

enlarged nuclei, defined as nuclei having a diameter greater than that of 10 micrometers (μm).[79]

Logistic regression model

Regression analysis uses information about a variable x to draw some type of conclusion concerning another variable y. The bivariate case involves only two variables, but analysis can be done on multivariate cases as well. Generally for biomedical purposes, and for the purpose of this study, the multivariate model is usually involved, and a dummy variable is also used. This dummy variable is simply a variable that is used to identify the classification group into which a particular data point belongs. For example, 1 can be used to identify dysplastic tissue sites and 2 to identify non-dysplastic tissues. Then using this variable and the appropriate parameters extracted from the spectroscopy, a probabilistic model can be computed. The logistic regression model is of the form

$$\ln \frac{p}{1-p} = a_0 + a_1 x_1 + a_2 x_2 + \ldots + e\,, \qquad /4.9/$$

where p is the probability of the event's occurrence (i.e. a particular data point belonging to group 1 or group 2), a are the coefficients of x, the independent variables, and e is random deviation. The logistic regression model is useful as it constrains the resulting estimated probability to lie between 0 and 1, and the calculation of this model is not computationally intensive. Using a calibration set of initial values, the coefficients for this model can be calculated and used to establish a threshold line or surface which is used to express that data points lying on either side of the surface belonging to a particular group with a certain probability p. This surface can then be used to assign classifications to a prospective data set for which the classification is unknown.

[79] Georgakoudi et al. (2001)

5
Results

Introduction

As already mentioned, a previous study had demonstrated that diagnostically useful information can be extracted and used for the detection of dysplasia in BE using TMS.[80] For such a technique to be clinically useful, data analysis has to be performed in real time, so that immediate feedback is provided to the physician, guiding him to areas that are likely to be diseased. To achieve this aim, a second generation FastEEM was designed and constructed. The main goal of this study was to confirm the original findings using spectra collected with this new instrument and to further develop and optimize diagnostic algorithms to be used as a real-time guide to biopsy. To accomplish this goal, a small set of spectra collected with the new FastEEM was studied and used as a calibration set. After this calibration, the results could be evaluated through prospective

[80] Georgakoudi et al. (2001)

data analysis, i.e. applying the diagnostic algorithms developed to a new, larger data set to validate the accuracy of the diagnostic thresholds.

The diagnostic algorithms would be based not only on the analysis performed previously, but would also include additional spectroscopic information provided by the second generation FastEEM. For example, the diagnostic potential of fluorescence spectra collected at 308 nm excitation could be assessed. As 308 nm is the excitation wavelength for tryptophan, the role of this fluorophore in the development of dysplasia could be studied to help understand in more detail the biochemical changes involved with dysplasia.

Along with tryptophan decomposition in the intrinsic fluorescence analysis, porphyrins also could be analyzed. In the previous study, spectra were decomposed into collagen and NADH contributions, while principal component analysis of IFS at 397 and 412 nm excitation suggested that porphyrin fluorescence could also be diagnostically useful.

Another aim was to focus on the real time aspect of the tool and to improve its speed. This could be done through optimizations in the data analysis code, in both syntactic optimizations and optimizations in program flow and design to minimize unnecessary calculations. This would allow for a more responsive program for the physician to use for guidance in taking biopsy samples.

Data set

The data used in this analysis consisted of over 500 sites from 168 patients undergoing routine surveillance for Barrett's esophagus at the Medical University of South Carolina. The measurements were taken over the span of two summers, 100 patients the summer of 2000 and the remaining 68 the summer of 2001. The patients' consent was obtained for all measurements, and the protocol used received approval from the Institutional Review Board of MUSC and the Committee on the Use of Humans as Experimental Subjects at the Massachusetts Institute of Technology. Biopsy samples were also taken from each of these sites so that a pathological diagnosis could be made to

verify the spectroscopic diagnoses. These pathologies were classified as high grade dysplastic, low grade dysplastic, non-dysplastic, or indefinite for dysplasia by two or three pathologists at both MUSC and the Children's Hospital Boston.

Of these data points, a subset of twenty-six data sites was taken to use as a calibration set, with fourteen non-dysplastic, four low grade dysplastic, and eight high grade dysplastic sites. Using this calibration set, the diagnostic algorithms developed in the previous study with the first generation FastEEM machine could be corroborated and any scaling discrepancies between the two FastEEM machines could be found and the algorithms adjusted as needed. After scaling, the remainder of the data could be used as a prospective set to verify the algorithms.

Analysis of calibration data set

Diffuse reflectance spectroscopy

As described previously, the initial step of the analysis involves a diffuse reflectance model fit to the measured reflectance spectra. Only by fitting the measured data to the model can the values of the parameters be determined that are then used in the

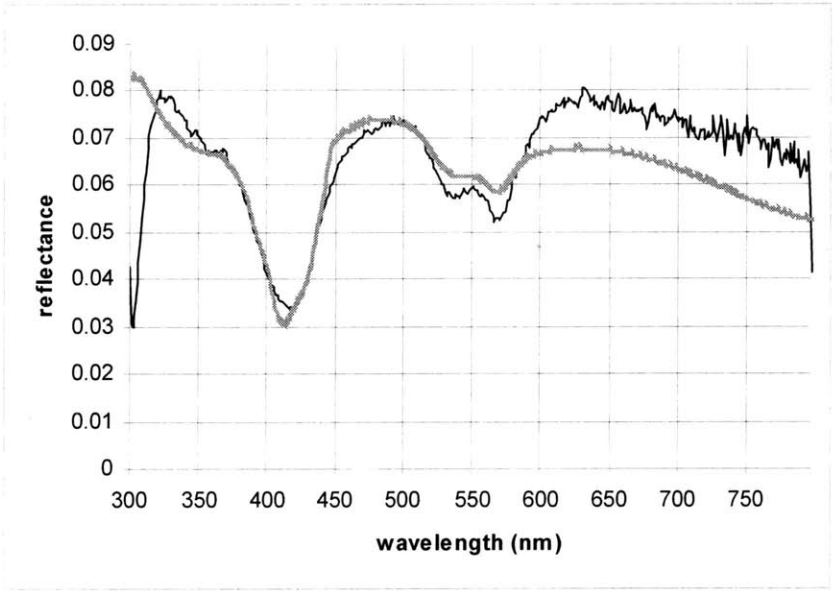

Figure 5.1: reflectance fit. Data in black, fit in gray.

diagnostic algorithms. In the earlier study, this fitting presented no problem, and the fits modeled the data reasonably well. For this calibration set, however, consistent discrepancies between the model and the data were clearly noticeable. Figure 5.1 shows a model fit of typical quality. It can be seen that at the long wavelengths, the portion that corresponds to the red part of the visible spectrum, the fit noticeably lies below the data.

Although the fits were not as good as expected, values of the diffuse reflectance model parameters seemed reasonable. The extracted wavelength dependent characteristics of the reduced scattering coefficient, μ_s', were consistent with those of the previous study. A linear fit to the coefficient data from the entire wavelength range was computed and extrapolated to calculate the slope and intercept of this fitted line. As shown in figure 5.2a, the slope and intercept of the line describing the wavelength dependence of μ_s' decrease with dysplasia, consistent with the original findings. The original data plot is shown in figure 5.2b, and while the scales on the two graphs and the ranges of the values are different, the consistency in trend is evident.

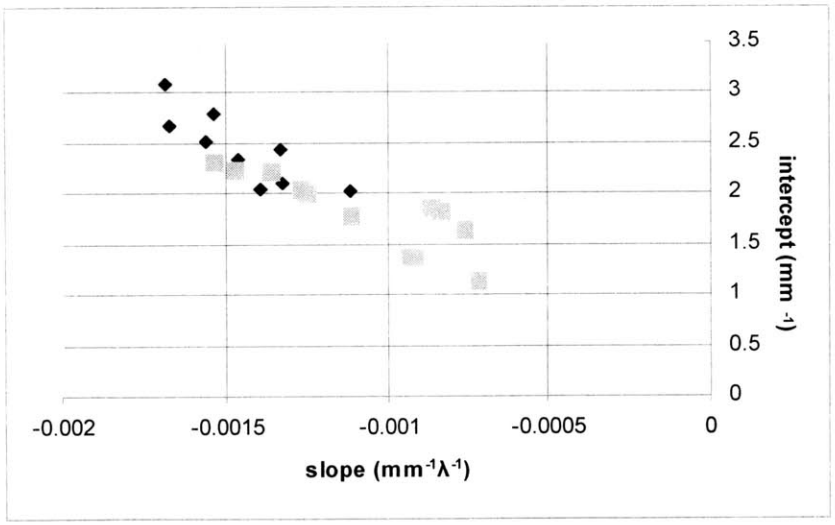

Figure 5.2a: black diamonds representing non-dysplastic sites and gray squares for dysplastic

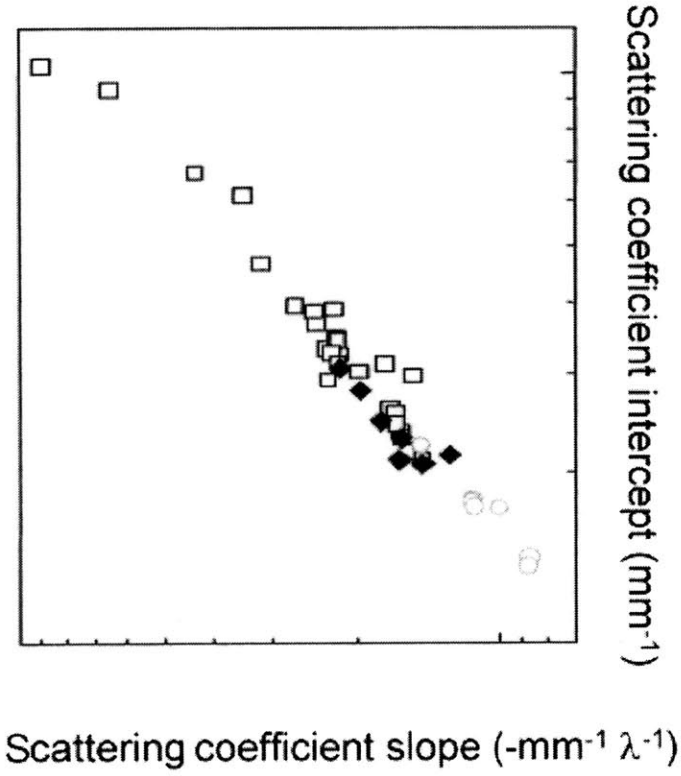

Figure 5.2b: plot from Georgakoudi et al (2000). Black squares non-dysplastic, filled black diamonds low grade dysplastic, gray circles high grade dysplastic.

Intrinsic fluorescence spectroscopy

At 337 nm excitation, the overall intensity lowers and shifts to the red region of the spectra as the tissue becomes more dysplastic. This shift in the peak indicates an increase in concentration of NADH and a relative decrease in collagen in the tissue. At 397 and 412 nm excitation, an increase in the relative intensity of the spectra in the red region correlated with dysplasia, consistent with an increase in porphyrin fluorescence. Fluorescence spectra exhibited similar changes with dysplasia as seen previously. Figure 5.3 shows the mean intrinsic fluorescence spectra at each of these excitation wavelengths are shown below, with the corresponding peak intensity normalized spectra, to highlight the lineshape differences.

Figure 5.3 (continued on next two pages)**:** intrinsic fluorescence spectra for 337, 397, and 412 nm excitation wavelengths. Non-dysplastic mean is in black, low grade dysplastic in dashed, and high grade dysplastic in gray.

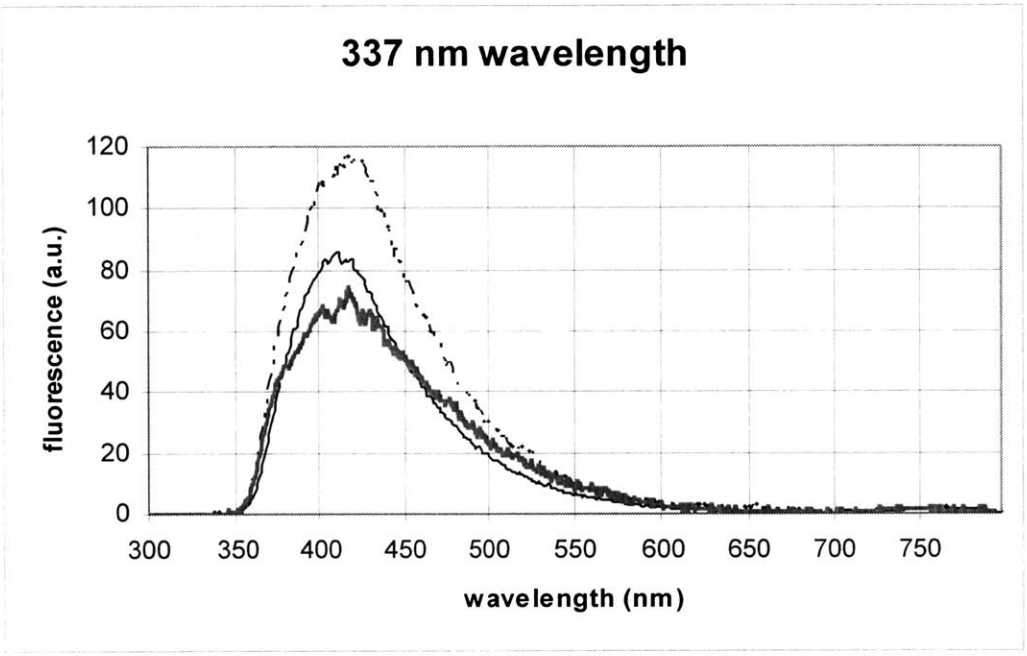

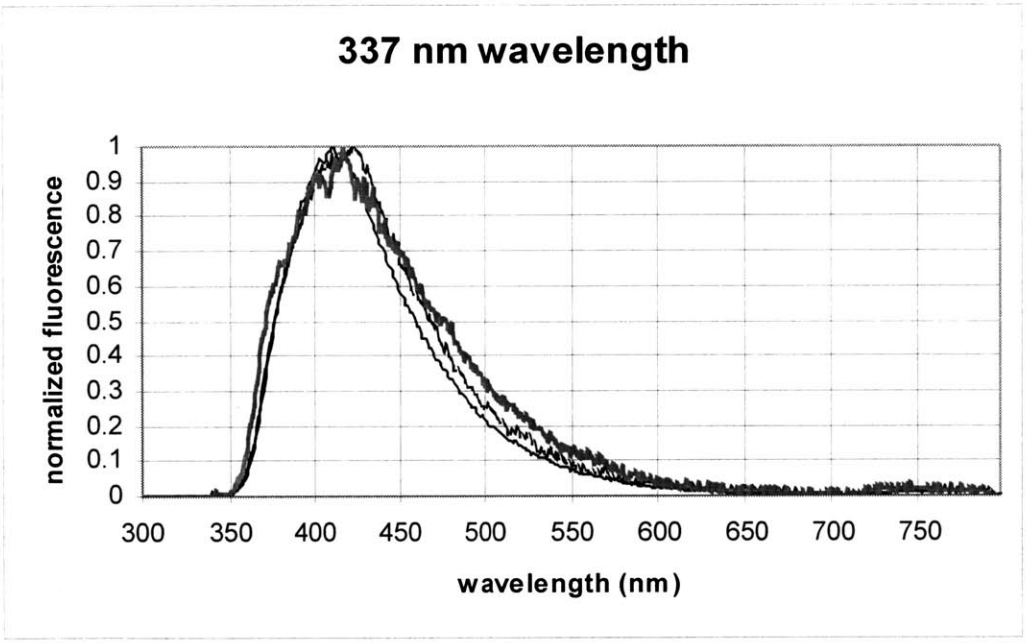

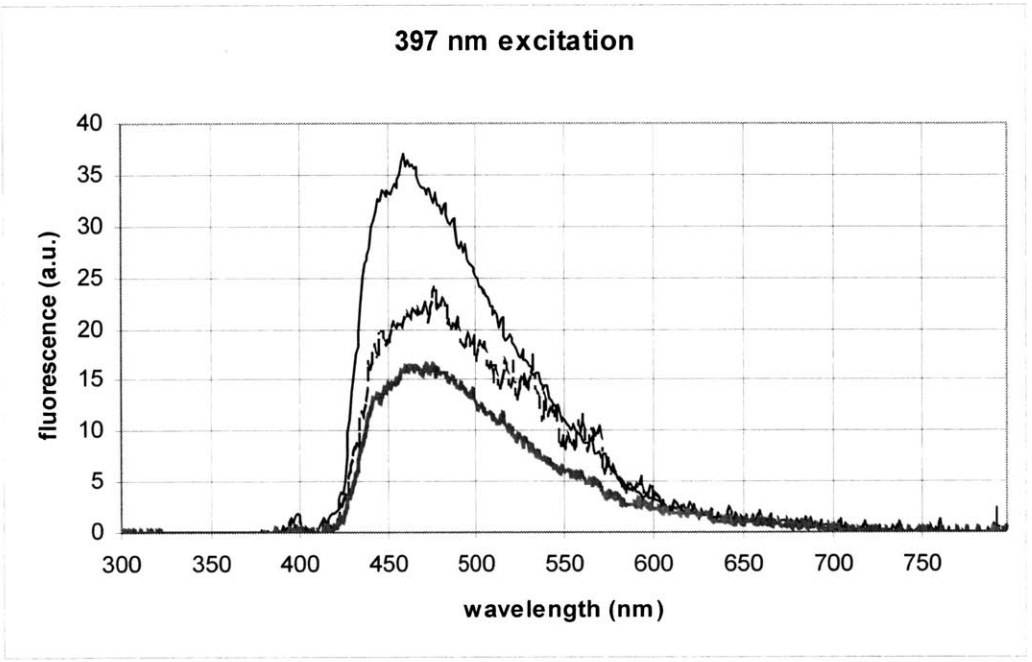

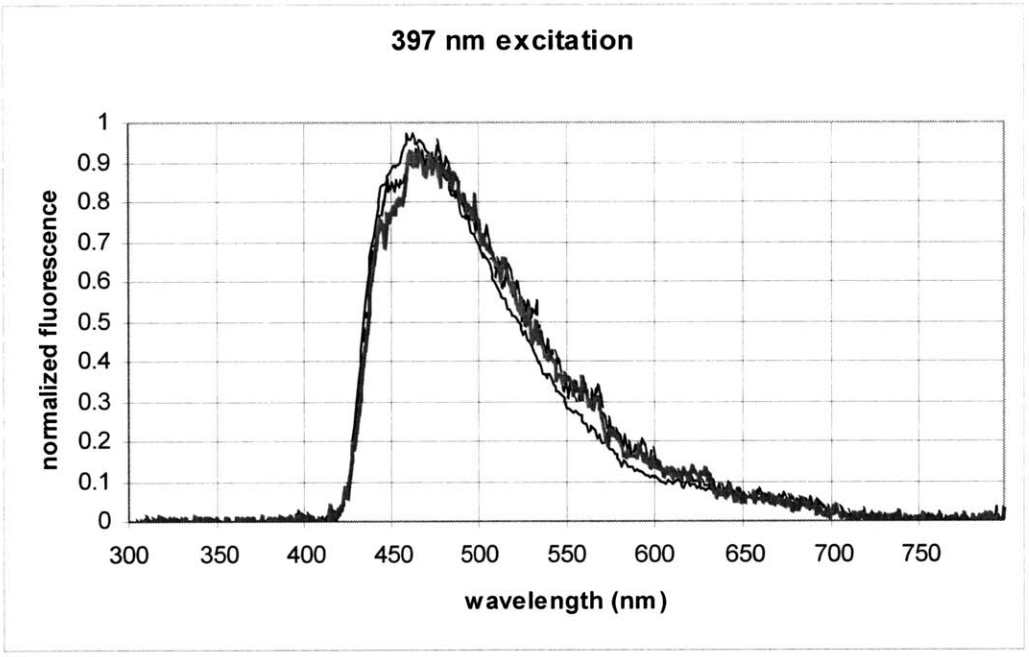

Figure 5.3: intrinsic fluorescence spectra for 337, 397, and 412 nm excitation wavelengths. Non-dysplastic mean is in black, low grade dysplastic in dashed, and high grade dysplastic in gray.

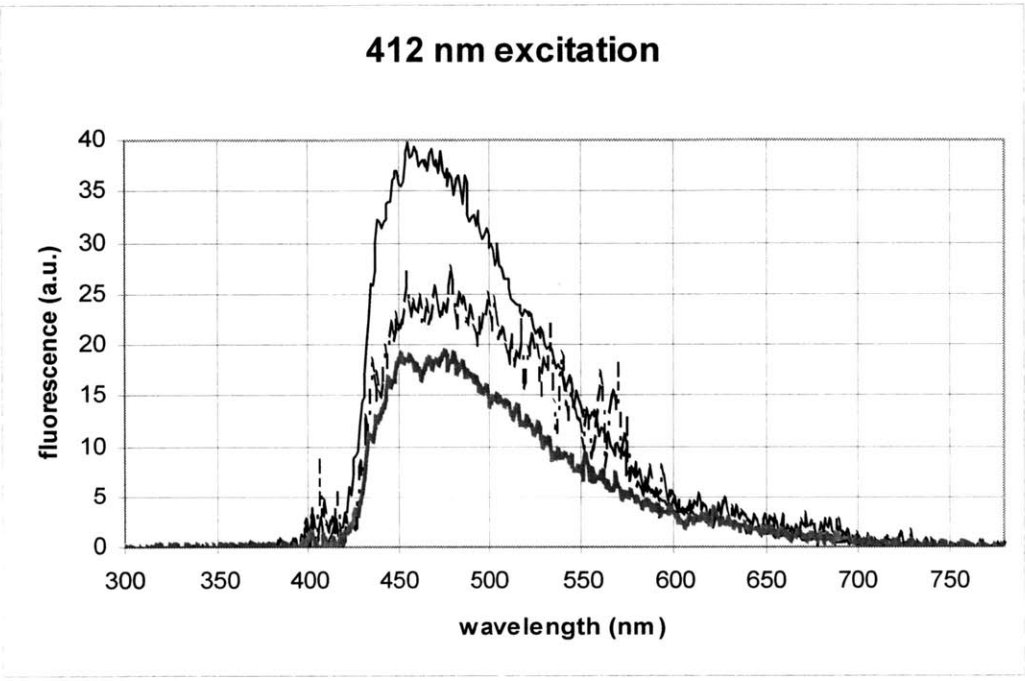

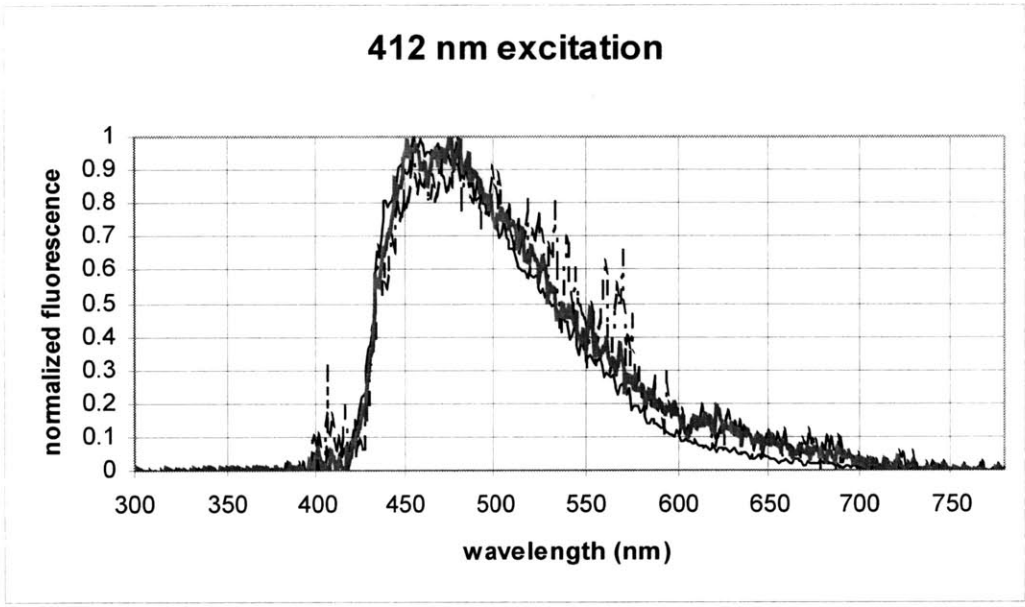

Figure 5.3 (continued from last two pages)**:** intrinsic fluorescence spectra for 337, 397, and 412 nm excitation wavelengths. Non-dysplastic mean is in black, low grade dysplastic in dashed, and high grade dysplastic in gray.

Light scattering spectroscopy

Analysis of LSS spectra had exhibited in the previous study the highest sensitivity and specificity for detecting dysplasia compared to IFS and DRS. Unfortunately, this is a technique that relies heavily on successful subtraction of the multiply scattered photon contributions to the measured reflectance spectra. This is achieved by subtracting the diffuse reflectance model fit from the measured spectra. Since problems in this initial analysis step were encountered, it was expected that those would limit the ability to perform LSS analysis. Indeed, as shown in Figure 5.4a, it is difficult to differentiate the three different types of tissue in any convincing manner. While the two high grade dysplastic triangles in the upper right are where they would be expected, the remaining dysplastic sites portray rather non-dysplastic results, more so than the non-dysplastic sites themselves. In contrast, figure 5.4b shows the LSS findings from the earlier study.

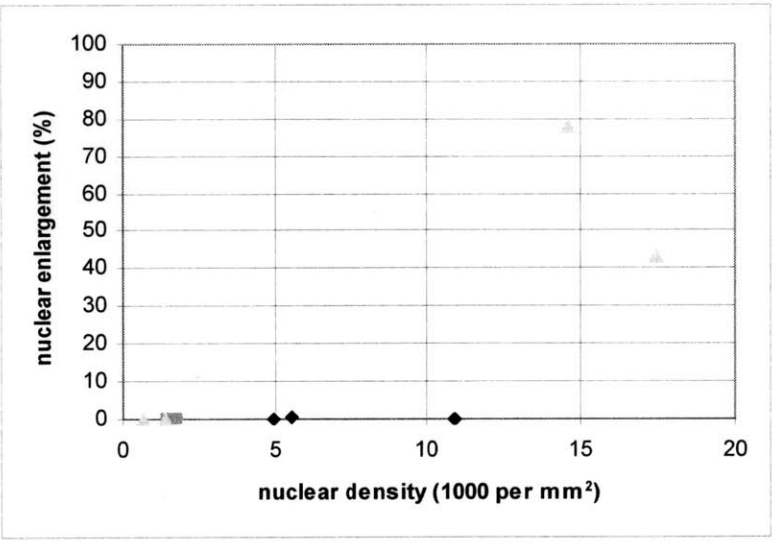

Figure 5.4a: results from LSS analysis. Non-dysplastic in black diamonds, low grade in gray squares, high grade in light gray triangles.

Figure 5.4b: plot from Georgakoudi et al (2000). Non-dysplastic in black squares, low grade dysplastic in filled black diamonds, and high grade dysplastic in black circles.

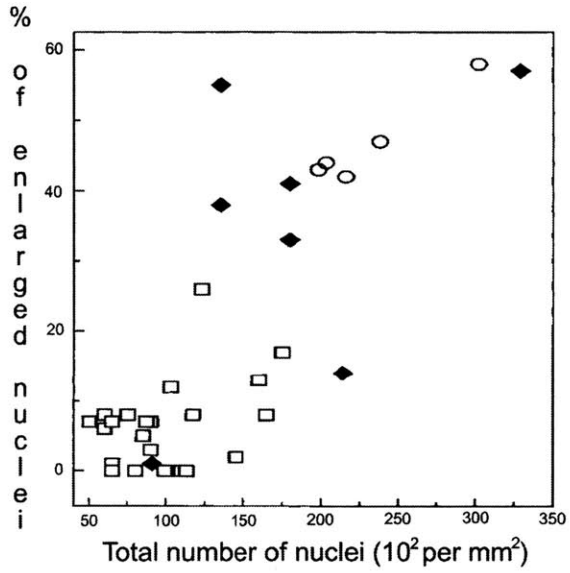

Another indication of the poor quality of the fits was the inability to extract an LSS analysis at all, regardless of its accuracy. The LSS analysis incorporated several checkpoints, in which the data is examined to ensure it is appropriately being modeled and the theory is being correctly implemented. For example, at one point in the data analysis, a second-order polynomial fit is made to the data, and this fit is compared to the diffuse reflectance fit. If these two fits are too similar, it is indicative that the modeled fit is not correctly accounting for hemoglobin absorption, and therefore, the LSS analysis is rejected. Such rejections, while a safeguard against incorrect diagnoses, were occurring far too frequently with this data set, with only nine sites yielding LSS spectra that could be analyzed. This was to be expected, with the consistently poor fits to the data. The only definite conclusion that could be drawn was the need to address the issue of the poor reflectance fits.

Solutions

This problem could be fundamentally approached in two ways. The first, and ideally better, solution would be to find the root cause of the discrepancy. This cause could be one or a combination of many different reasons—optics distortion problems and background calibration problems are just two possibilities. The second solution would be more of a "quick fix," finding a way to take the measurements as they are and applying some sort of algorithm that would make it correspond to the proper diagnosis. The focus of this thesis is the latter solution. While more superficial than the first, the advantages to this solution are many, the most obvious of which is the difference in time scale. But perhaps more importantly, this second solution may be of great guidance in discovering the root problem, and devising a more permanent solution. It may also very well be the case that even when the deeper problem is discovered, the solution is not feasible or practical to implement, in which case this quick fix will be a necessary component in the use of this tool.

A number of approaches were explored that could potentially improve the quality of the diffuse reflectance model fits, and, thus the quality of the LSS spectra. The first approach employed was to relax the restrictions placed on the allowed values of diffuse reflectance fitting parameters when calculating the best fit to the data. The idea behind this would be that while it might make the parameters for the reflectance slightly less physically accurate, this sacrifice would be made up for by the more accurate light scattering analysis. Any loss in the direct reflectance analysis could be avoided by doing two fits, one for the purpose of extracting direct reflectance parameters, and the second for extracting light scattering parameters. The obvious drawback would be the increased time needed for the analysis, but computation time could be improved in other ways.

Additionally, the effects of optimally fitting distinct spectral regions, such as the 415 nm hemoglobin absorption region, on the quality of the extracted LSS spectra were also explored. In determining the best fit to the data, the error between the data and the model is weighted so as to preferably minimize discrepancies in certain spectral sections. The sections that are more or less heavily weighted and how much they are weighted were manipulated to improve the fits.

The results of this approach, however, forewent any further need for considering the tradeoffs between time and accuracy. While the fits were improved remarkably, the LSS results were still inconsistent. Figure 5.5 shows a sample of the improved

Figure 5.5: data in black, old fit in dark gray, new fit in light gray.

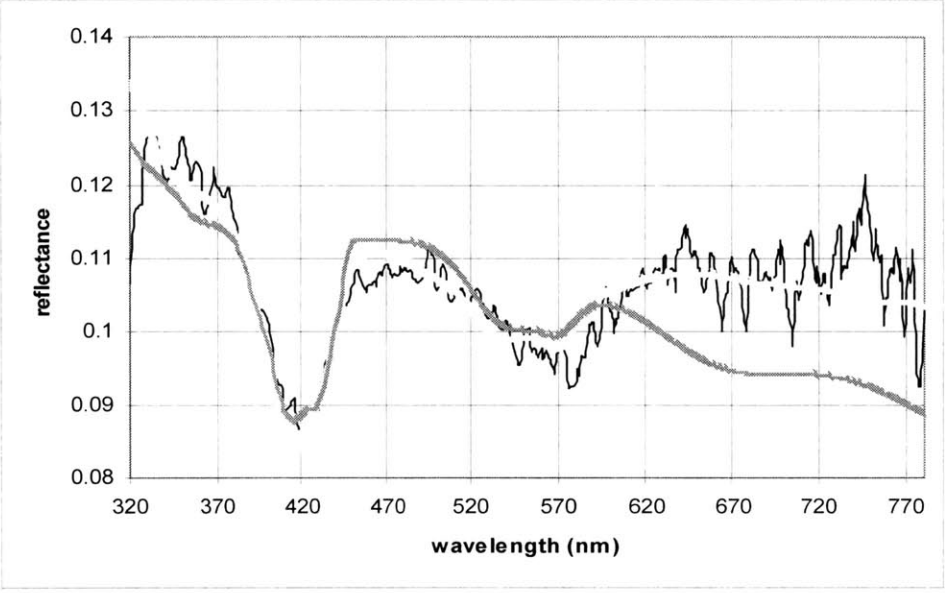

reflectance fit, compared with the original, unrelaxed parameter fit. The resulting scatter plot comparing the nuclear density and enlargement for all the calibration data set is shown in figure 5.6. With the improved fits, a larger percentage of the sites provided LSS spectra, fifty percent, as opposed to the forty from the original fits. Although the accuracy of the information seems slightly improved, distinction of dysplastic progression could not be made.

Another solution came about while examining the raw data from the measured

Figure 5.6: black diamonds non-dysplastic, gray squares low grade dysplastic, and light gray triangles high grade dysplastic

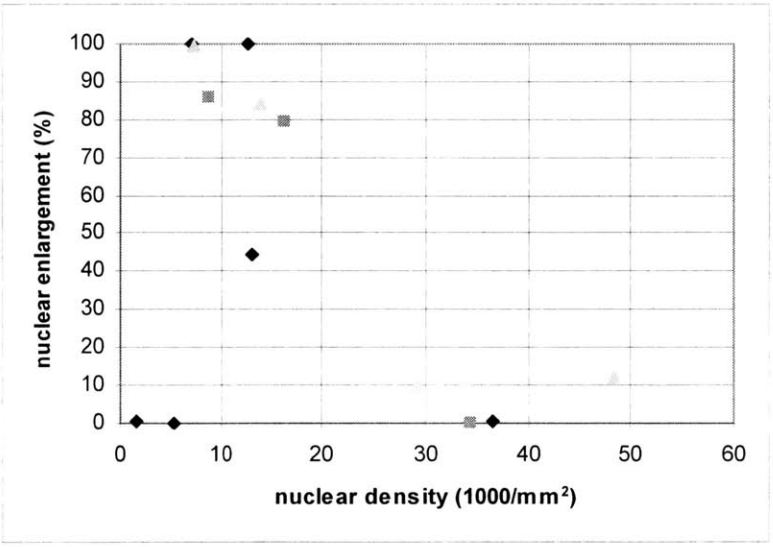

spectra. Looking for commonalities between the spectra that provided good fits versus those that resulted in poor ones, one characteristic seemed to be that the relative intensities of the data and the backgrounds were significantly higher in those that resulted in good fits. This seemed to imply the importance of a good signal to noise ratio in the measured data. In an attempt to artificially improve this ratio, the effect of subtracting either fractions or multiples of the measured background from the measured reflectance was examined (figure 5.7). This would affect the signal to noise ratio by increasing the remaining intensity of the spectra. This is true because the background is subtracted from both the measured reflectance and the white standard, and the intensity is a ratio of these two.

Figure 5.7: original fit on top, same as Figure 5.1, same data with double the background subtracted below. Dark line is data, lighter line is fit.

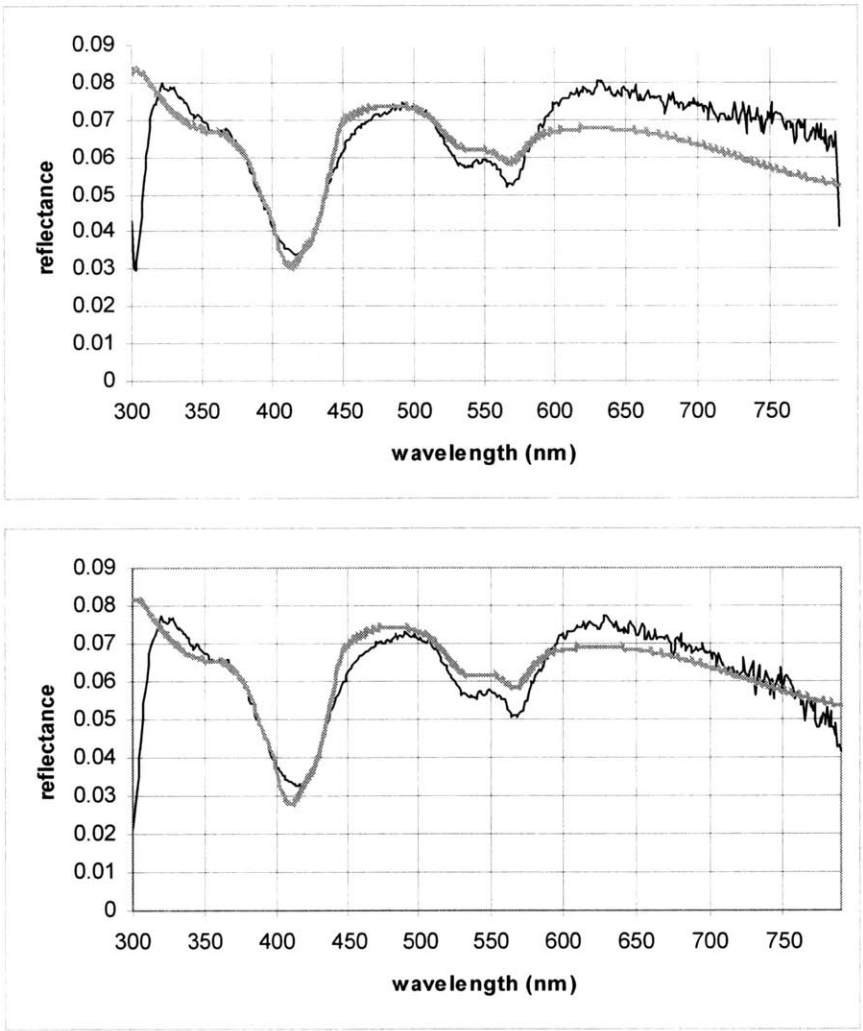

As learned from the first approach, an improved fit does not necessarily result in a more accurate LSS analysis. The result was no different with the manipulation of the background. None of the constants used for scaling the background produced a consistently accurate light scattering spectrum.

To gain a better understanding of the origins of the discrepancy between the reflectance model and the measured data, a series of diffuse reflectance measurements were performed using physical tissue models, or phantoms, that consisted of water, polystyrene beads (1 μm in diameter) and hemoglobin. The concentration of beads was varied to simulate μ_s' in the physiologically relevant range between 0.5 and 6 mm^{-1}. The hemoglobin concentration was varied between 0 and 2 g/l to simulate physiological ranges of μ_a. Fits of the model to reflectance spectra acquired from such models exhibited a similar discrepancy in the red region of the spectra as that seen for the *in vivo* reflectance fits. These phantom measurements also indicated that the deviation between model and data was dependent only on the μ_s' value, not on μ_a. Specifically, the smaller the value of the μ_s' was, the higher the deviation. Based on the phantom measurements, a μ_s' dependent correction surface was developed, in which the modeled reflectance was multiplied by a correction factor at each wavelength, which depended on the value of the fitted μ_s'. As shown in figure 5.8, this correction factor increases in the red region of the spectrum, and it becomes higher as the μ_s' decreases.

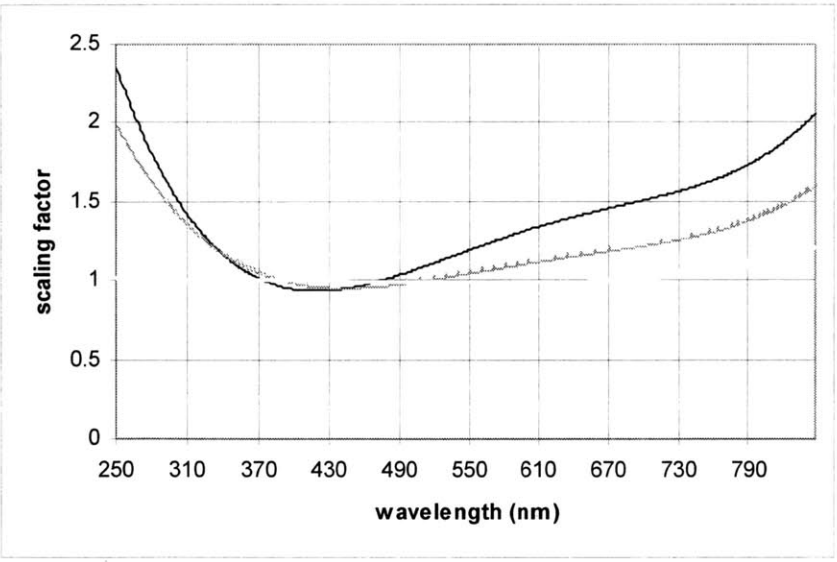

Figure 5.8: the black line corresponds to μ_s' values of 0.52, the dark gray line to values of 1.32, light gray, 4.47. Correction factors for intermediate mus' are interpolated based on these curves.

A further modification involved the look-up table that is used during the fitting routine to estimate the value of μ_s' at different wavelengths based on the fitted parameter values for scattering particle size and density. For example, looking at the scattering cross section for a particle with a diameter of 1.7 μm, it exhibits strong wavelength dependent oscillations. Previous studies suggest that the tissue μ_s' is a smooth monotonically decreasing function of wavelength. Thus, to better approximate the physiological characteristics of μ_s', the scattering cross sections corresponding to different scattering particle sizes given by Mie theory were replaced by their corresponding second order polynomial fits. Figure 5.9 illustrates this adjustment.

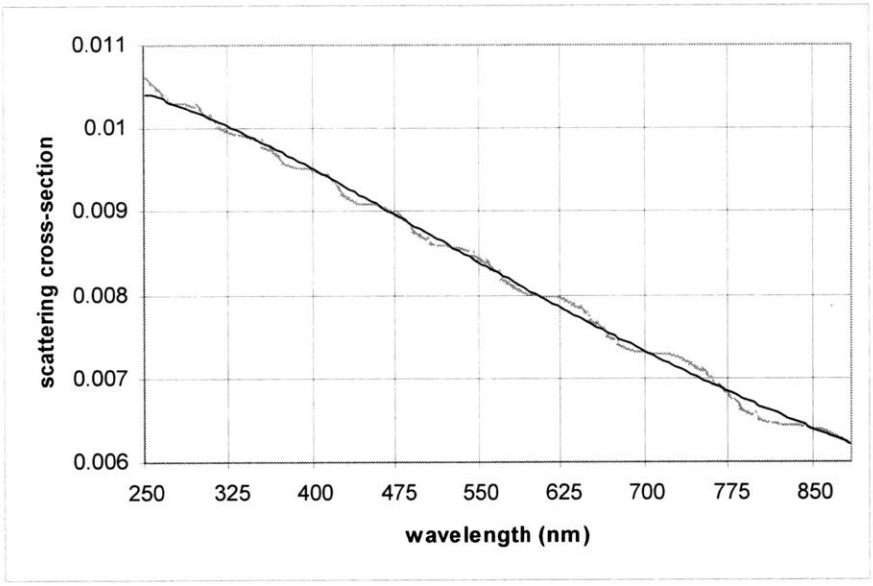

Figure 5.9: gray line indicates former Mie surface, smoother black line represents new surface, both showing scattering cross sections for particles with radii of one micron.

In addition to exploring the possibilities of scaling the model fit, the program used to extract the light scattering spectrum itself was also assessed to ensure there were no bugs in the code. Upon inspection, a few areas in which improvements were required were identified. For example, one of the checkpoints mentioned checks to ensure that there is a dominant frequency in the Fourier transform of the LSS spectrum. Circumstances in which either a false negative or a false positive could pass through this checkpoint were discovered. The code was modified to assess the form of the Fourier transform in a more rigorous way. Such implementation errors were found and

debugged, and at the same time, minor optimizations were made to clarify the code and decrease program runtime.

Analysis of recalibration data set

Using the modifications to the Mie surface and the μ_s' dependent reflectance intensity correction factor (figure 5.8), new fits were made to the data set in order to achieve the original goal of calibrating the algorithms to the new machine. These new fits were significantly better than the fits that were being returned with the original calibration set. Figure 5.10 shows the clear difference in the quality of the fit, especially in the red region where the original fit was unable to model the data correctly.

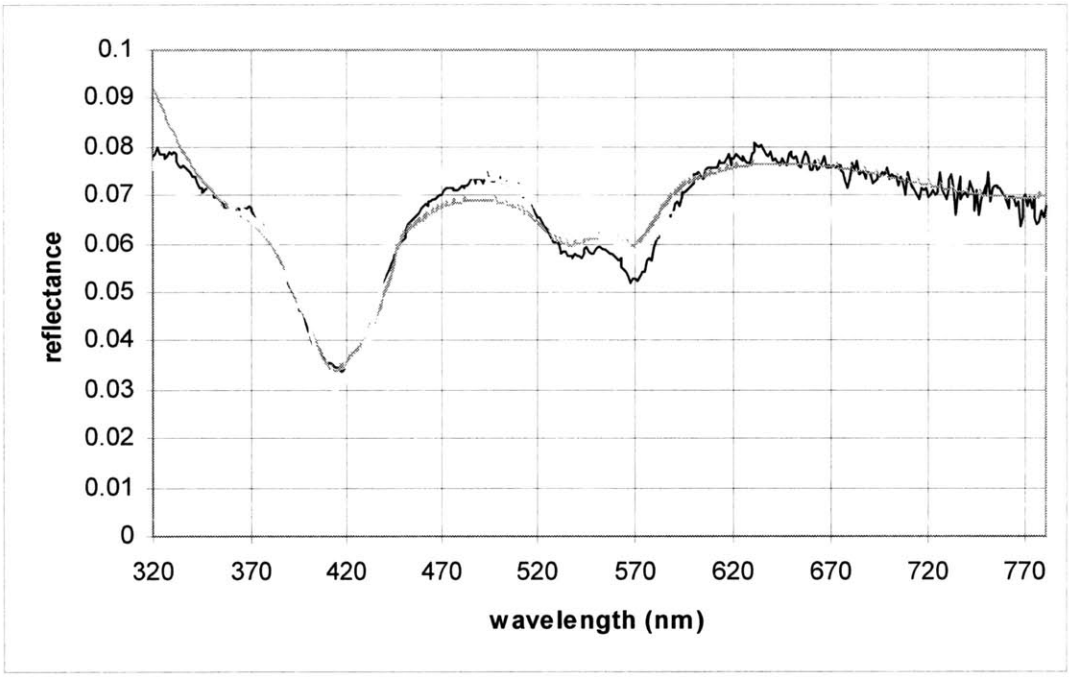

Figure 5.10: data in black, new fit dark gray, old fit light gray.

Using these improved fits, the data was analyzed as a calibration set for developing diagnostic algorithms once again.

Diffuse reflectance spectroscopy

The fitted magnitudes of the reduced scattering coefficients at 600 nm for the data showed a clear distinction between non-dysplastic and dysplastic tissue sites. Looking at the slope and intercept of the wavelength dependent μ_s' data, however, the differences were not as clear. Figure 5.11 shows the differentiation that can be made looking at intensities, where non-dysplastic is overall generally higher, compared with the inconclusive data of the slope and intercept. It seems as though the incorporation of the wavelength dependent correction factor interfered with the capability to extract reliably the slope of the μ_s'.

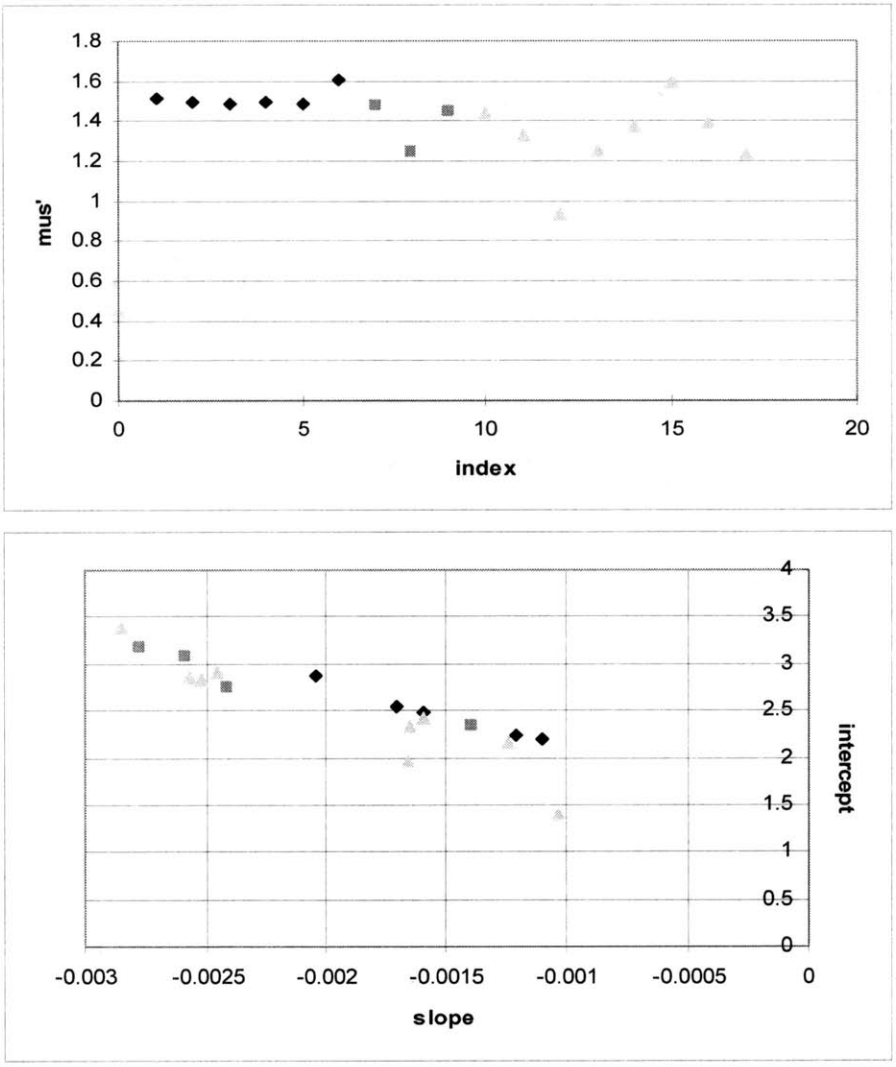

Figure 5.11: μ_s' values at 600 nm plotted above, slope vs. intercept below. Non-dysplastic in black, low grade gray, and high grade light gray.

Although these parameters of slope and intercept of the μ_s' were the primary ones used in the previously developed algorithm, they are not the only parameters returned and the only information that diffuse reflectance spectroscopy provides. As explained previously, there is also an absorption parameter that provides information about the hemoglobin concentration, as hemoglobin is the dominant absorber in the visible wavelength range. The hemoglobin concentration could also be used to detect dysplasia, as it has been found to be a diagnostically useful parameter in the detection of adenomatous colon polyps.[81] Looking at the Hb concentration, along with the intensity of the reduced scattering coefficient at 600 nm, a much more diagnostically useful pattern can be seen in the data, as shown in figure 5.12. The decision lines were drawn using logistic regression.

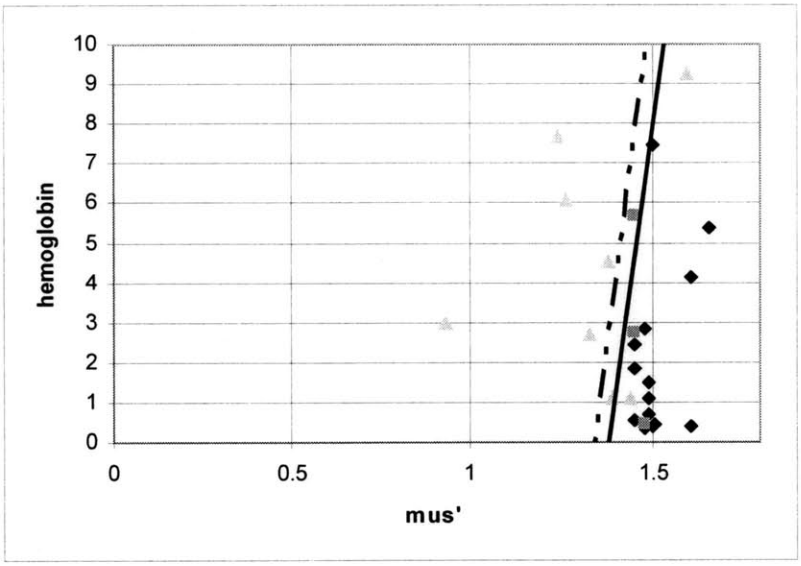

Figure 5.12: black diamonds non-dysplastic, dark gray squares low grade, light gray triangles high grade. Solid line is logistic regression line dividing dysplastic from non-dysplastic, dotted line separates high grade from the other two.

[81] Zonios et al.

Although this departs from the originally developed algorithm, its consistency with this recalibration data set is undeniable, and its validity can be verified through the prospective data analysis.

Intrinsic fluorescence spectroscopy

The modifications implemented in the analysis of the diffuse reflectance spectra did not affect in any significant way either the lineshapes or the intensities of the corresponding intrinsic fluorescence spectra. Figure 5.13 shows the characteristic shifts and changes in intensity seen at 337, 397, and 412 nm excitation wavelengths.

The intrinsic fluorescence spectra excited at six wavelengths between 337 and 425 nm were further decomposed into NADH and collagen contributions, using a linear least squares fitting algorithm, with NADH and collagen basis spectra extracted from a previous study as described in chapter four.[82] A general trend can still be seen (figure 5.14), especially between the high grade dysplastic and the non-dysplastic sites. The dysplastic tissue plots are found more to the upper left, indicating as expected with the biochemistry, an increase in NADH concentration and decrease in collagen concentration with the development of dysplasia. The low grade dysplastic measurements were not as clear, which is not surprising. Two lines were drawn using logistic regression to compute diagnostic thresholds using these points. The solid line is to separate non-dysplastic sites from dysplastic, both low grade and high grade. The dashed line is to separate high grade dysplastic from the other two. These lines are used to diagnose the prospective data set before corroborating them with the pathologic diagnosis. These prospective results are given later in this chapter.

[82] cancer paper

Figure 5.13 (continued on next two pages)**:** intrinsic fluorescence data. Black line non-dysplastic, dashed line low grade dysplastic, gray line high grade dysplastic

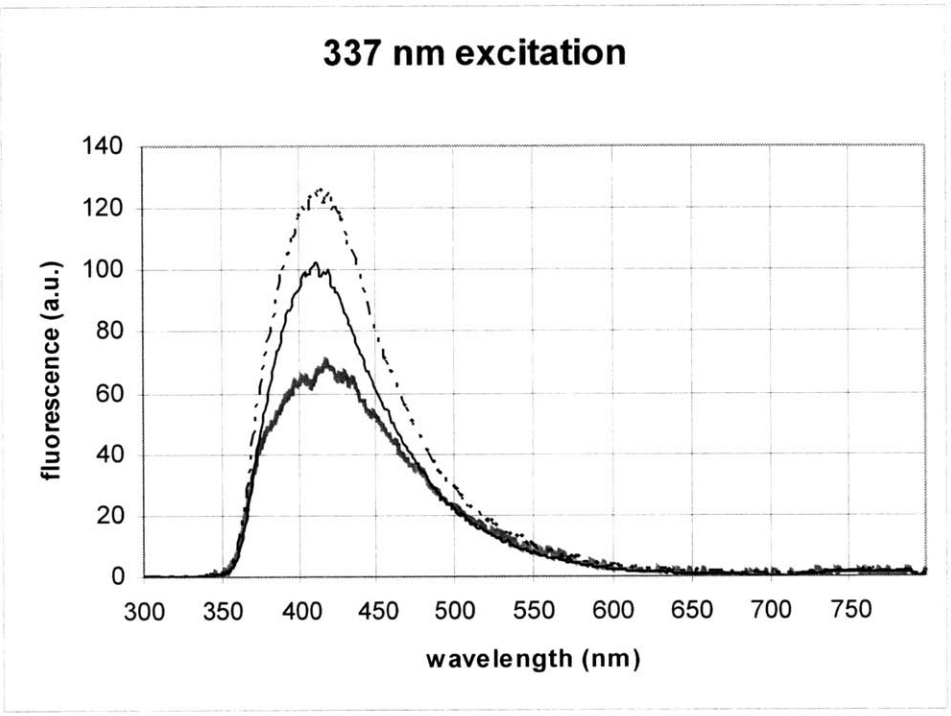

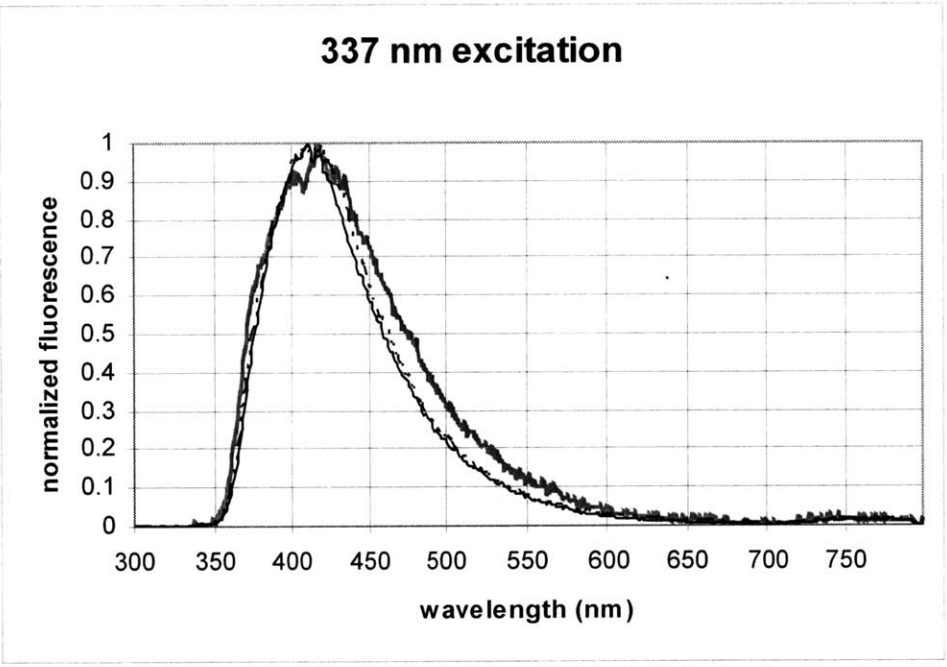

Figure 5.13: intrinsic fluorescence data. Black line non-dysplastic, dashed line low grade dysplastic, gray line high grade dysplastic

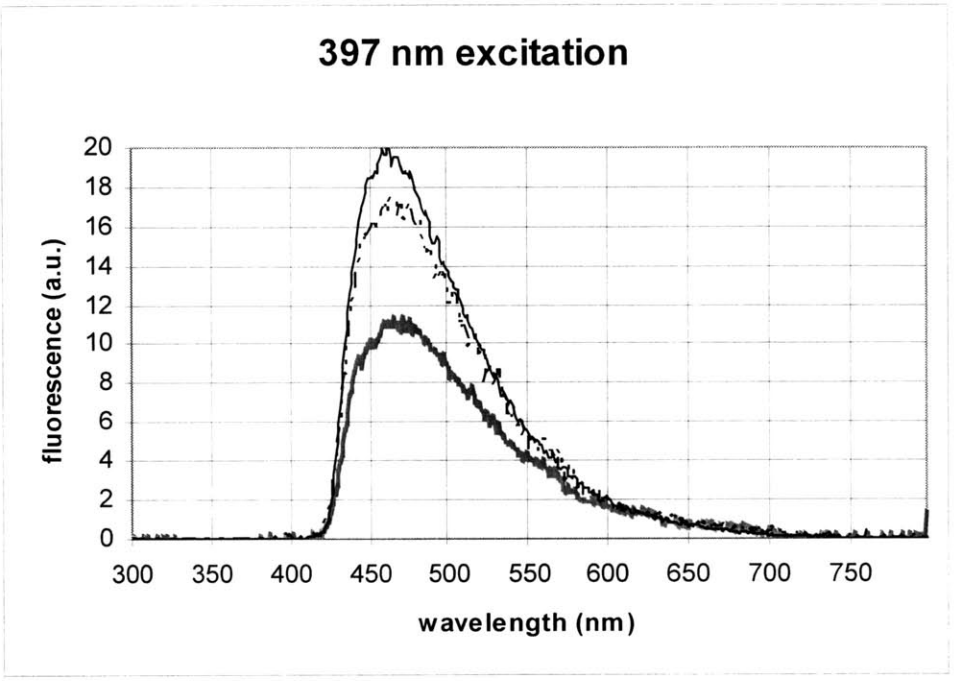

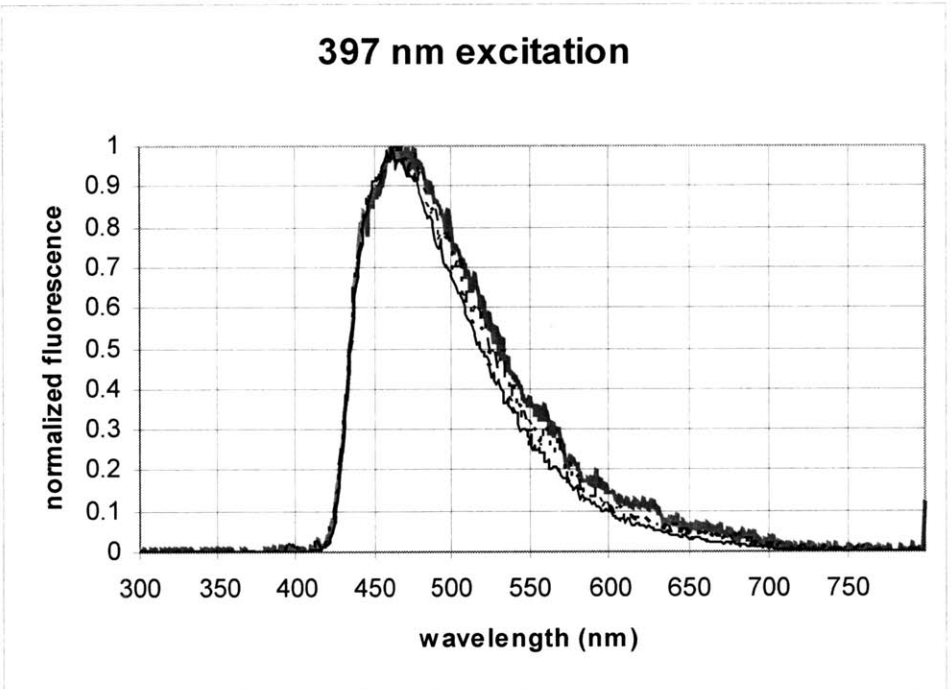

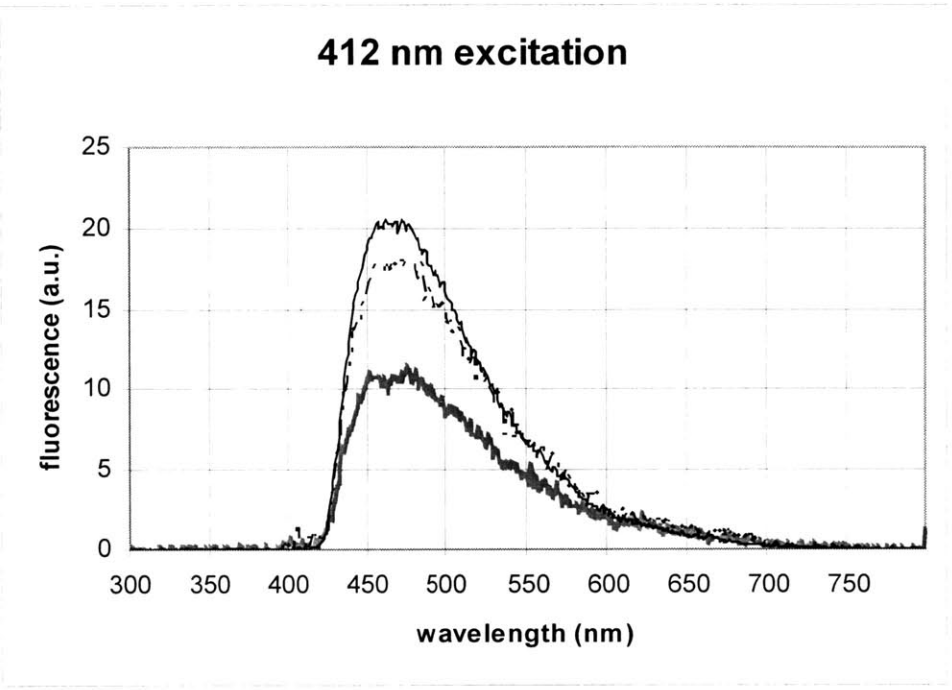

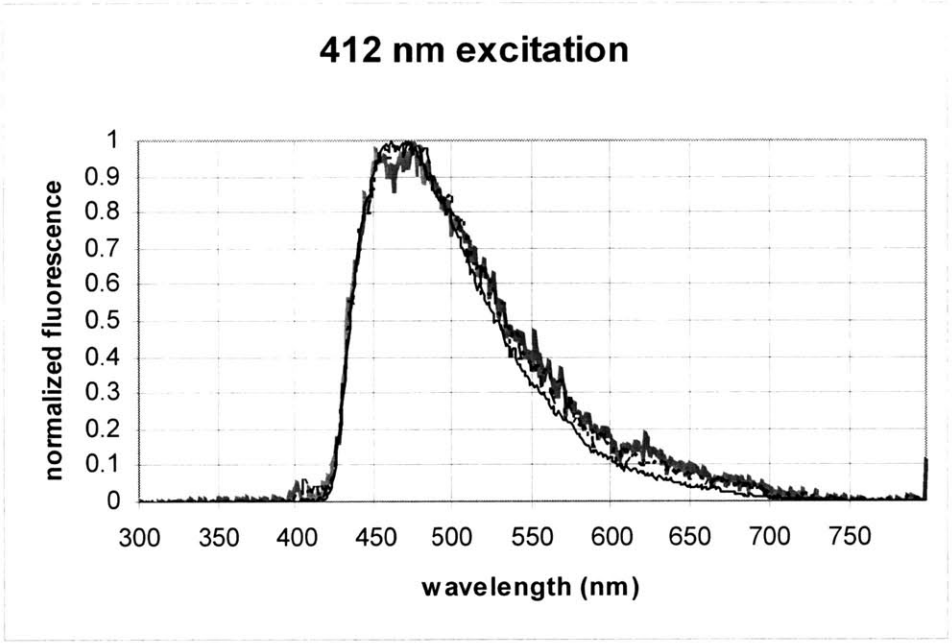

Figure 5.13 (continued from previous two pages)**:** intrinsic fluorescence data. Black lines non-dysplastic, dashed lines low grade, light gray lines high grade.

Figure 5.14: intrinsic fluorophore decomposition. Solid line for non-dysplastic and dysplastic, dashed line for high grade and non-high grade

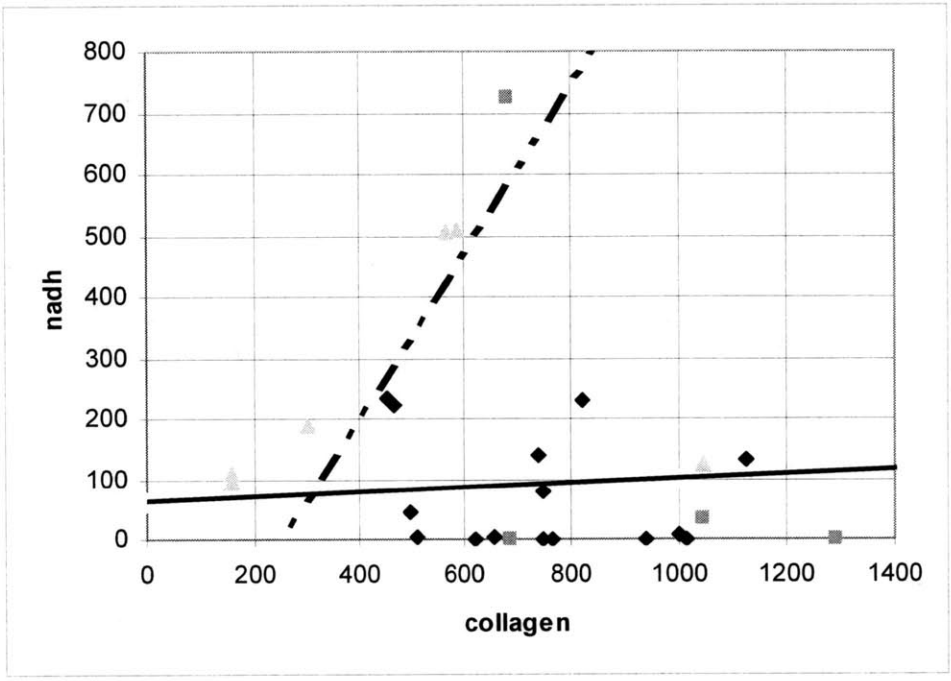

To make this decomposition algorithm more effective, porphyrin spectra were also examined at 397 and 412 nm excitation wavelengths, where the dysplastic spectra displayed a relative increase in intensity in the red region. The porphyrin spectra were experimentally extracted from these spectra using multivariate curve resolution. These extracted spectra were then reapplied to decompose the remaining 397 and 412 nm fluorescence spectra into porphyrin and collagen concentrations.

In figure 5.15, there can be seen a relatively clear distinction between the non-dysplastic characteristics and the dysplastic characteristics. The non-dysplastic sites have the higher collagen concentrations and lower porphyrin concentrations as the fluorescence spectra indicated, and the high grade dysplastic sites display the opposite features.

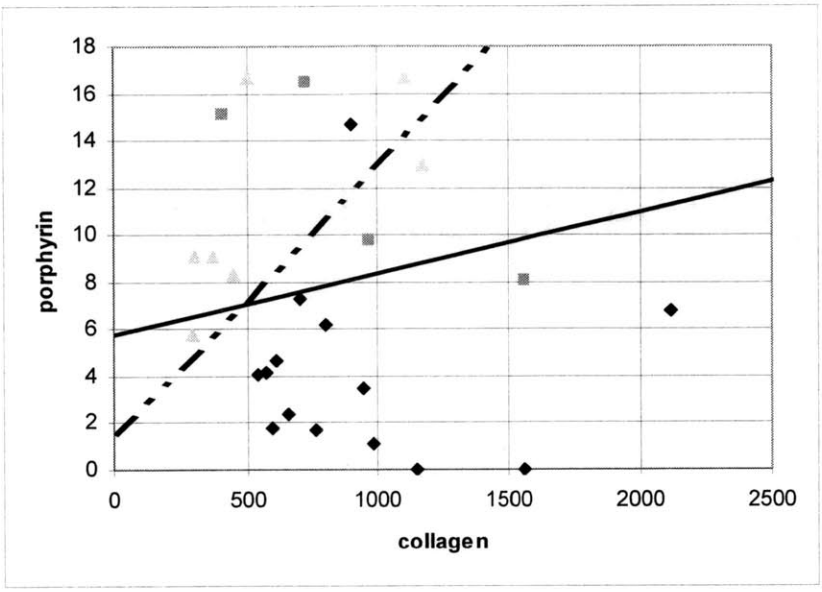

Figure 5.15: fluorophore decomposition, black diamonds non-dysplastic, dark gray squares low grade, light gray triangles high grade. Solid line non-dysplastic vs. dysplastic, dotted line high grade vs. other.

One last fluorophore could be used in decomposition, the previously unexamined tryptophan fluorescence in the 308 nm excitation wavelength. The mean intrinsic fluorescence spectra at this excitation can be seen in figure 5.16. At this wavelength, the contributing fluorophores are collagen and tryptophan. The collagen contribution is in the 400-500 nm emission range, while tryptophan fluoresces in the lower 300 nm range. The relative peak intensities are reversed, as tryptophan concentration increases in dysplastic tissue, resulting in the higher peak intensities for dysplastic spectra. The shift in the spectra is found in the normalized curves in the 400-500 nm range, the collagen differentiation, where the three curves clearly delineate themselves from each other when they so closely overlapped before and after this range. This consistency with observed biochemistry makes this new excitation wavelength another promising one to improve the diagnostic algorithm. Extracting the tryptophan spectra as done with the porphyrin spectra, the decomposition of the fluorescence spectra yielded results as expected. Figure 5.17 shows the decomposition into tryptophan and collagen components.

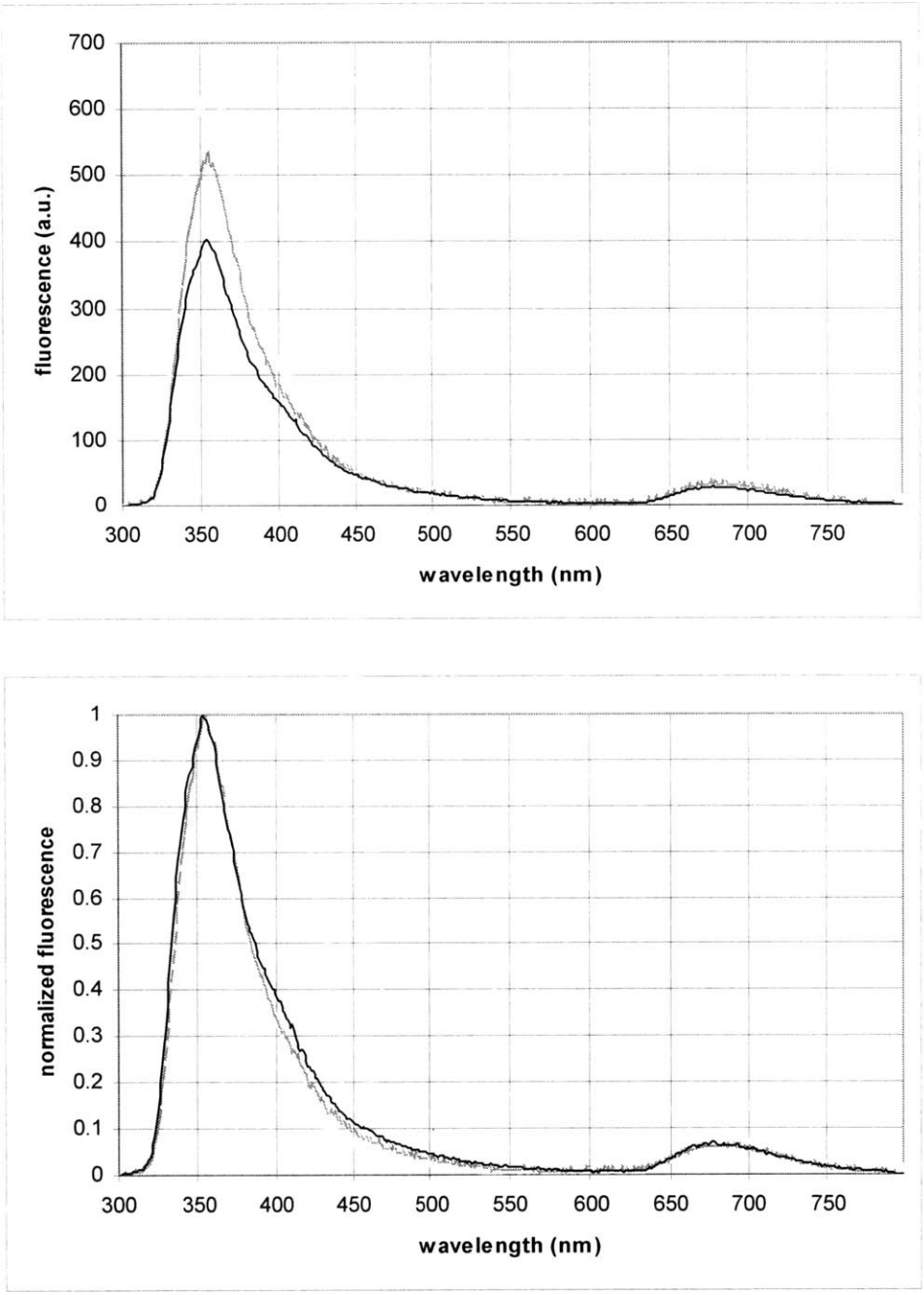

Figure 5.16: intrinsic fluorescence spectra for 308 nm excitation. The small peak found at 680 nm is the result of second order effects, reflecting the first order peak at 340 nm.

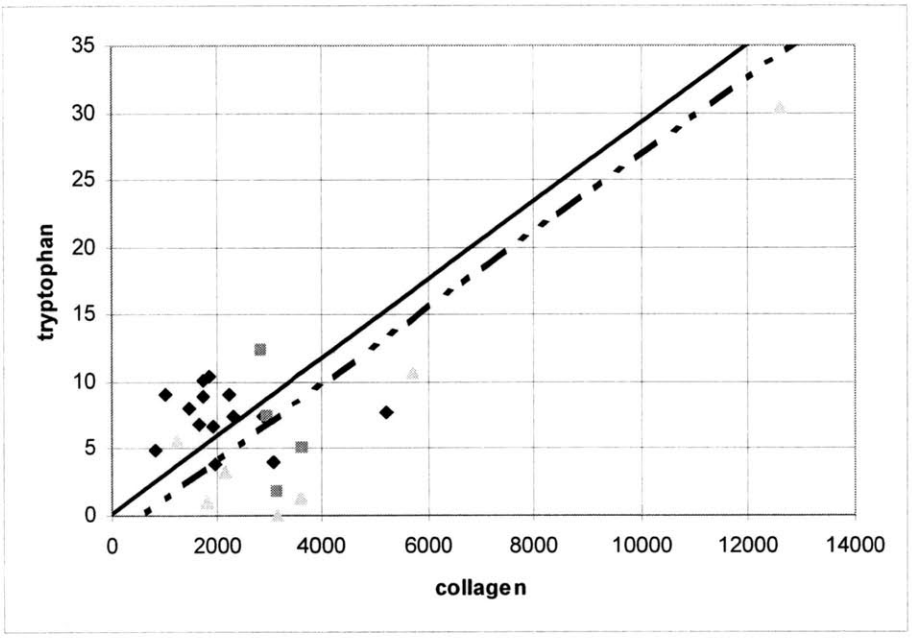

Figure 5.17: black diamond non-dysplastic, dark gray square low grade, light gray triangle high grade, solid line dysplasia division, dashed line high grade division

As the differences were clear in the fluorescence spectra, the decomposition result shows a clear delineation especially between non-dysplastic and dysplastic tissue sites.

Combining, then, three of the fluorophore concentrations into one three-dimensional plot would improve the differentiation between the different types of tissue. As the collagen, porphyrin, and tryptophan decompositions gave the most promising results, these three were used for the three-dimensional plot. The resulting figure is shown on the following page. These plots differentiate very clearly between the three types of tissue. NADH was also incorporated for a four-dimensional decision surface, using the resultant equation to diagnose, but the results were no better than the three-dimensional plots shown.

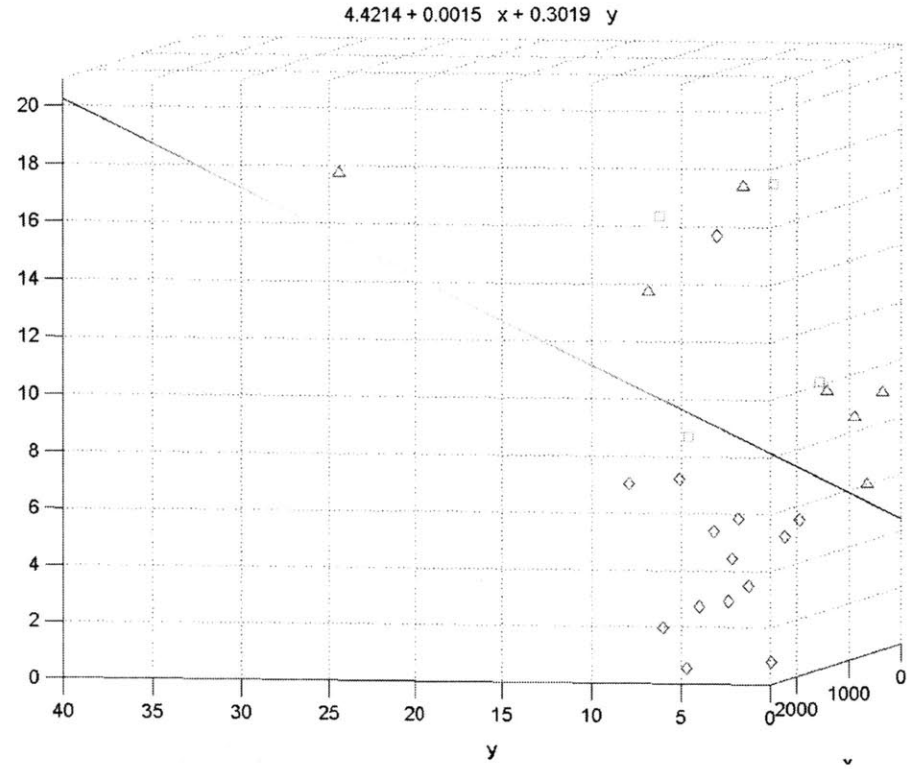

Figure 5.18: non-dysplastic in blue diamonds, low grade in green squares, high grade in red triangles. Above divides dysplastic from non, below high grade from non. X-axis is collagen, y-axis tryptophan, and z-axis porphyrin

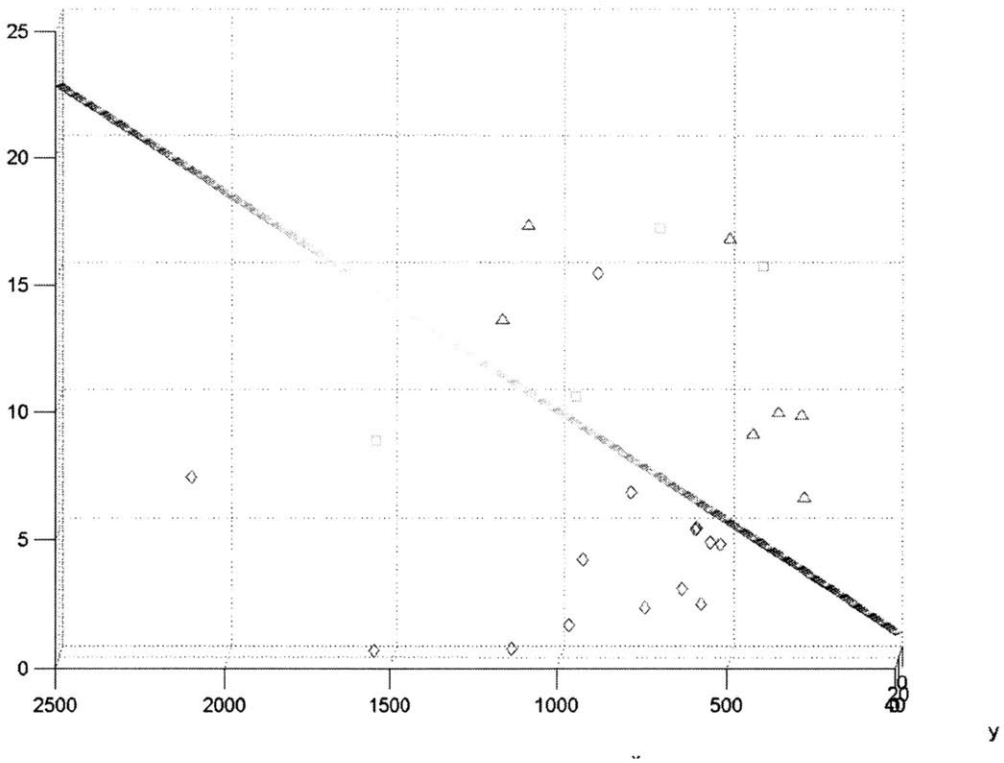

As with tri-modal spectroscopy as a whole, the combination of three techniques shows a drastic improvement over any of the four techniques alone. The exact figures for the results of this combined intrinsic fluorescence analysis are given in table 5.1, with the analysis of the other two spectroscopy types and the tri-modal spectroscopy results.

Light scattering spectroscopy

Finally, the light scattering spectra were analyzed, and the results were far clearer than found previously in the initial calibration set. From figure 5.19, although the yield of only half the points was lower than expected, the dysplastic development can be readily distinguished. Along with the nuclear enlargement and density parameters returned before, the analysis was also modified to return a distribution width parameter, which correlates to the range of nuclear sizes found in the tissue sample. Using these three parameters, three different plots were made, plotting two at a time. Each one had clear thresholds of differentiation between dysplastic and non-dysplastic. It seems with the improved reflectance fits drawn with this new Mie correction surface, the LSS algorithm can again be effectively applied. Although the delineations are quite clear, the high grade versus low grade and non-dysplastic threshold was not as effective, as the low grade dysplastic sites seemed to display the dysplastic characteristics to a greater magnitude than the high grade dysplastic (figure 5.19). This greater effectiveness in diagnosing dysplastic from non-dysplastic for light scattering spectroscopy, however, is consistent with what was found previously.[83]

Tri-modal spectroscopy

With these newly modified diagnostic thresholds for each of the three types of spectroscopy, the three types can again be combined to be used as tri-modal spectroscopy. The preliminary study took a simple majority diagnosis among the three

[83] Georgakoudi et al. (2001)

spectroscopy types, with effective results, and the same was done for the calibration set. The results from the calibration set can be seen in table 5.1.

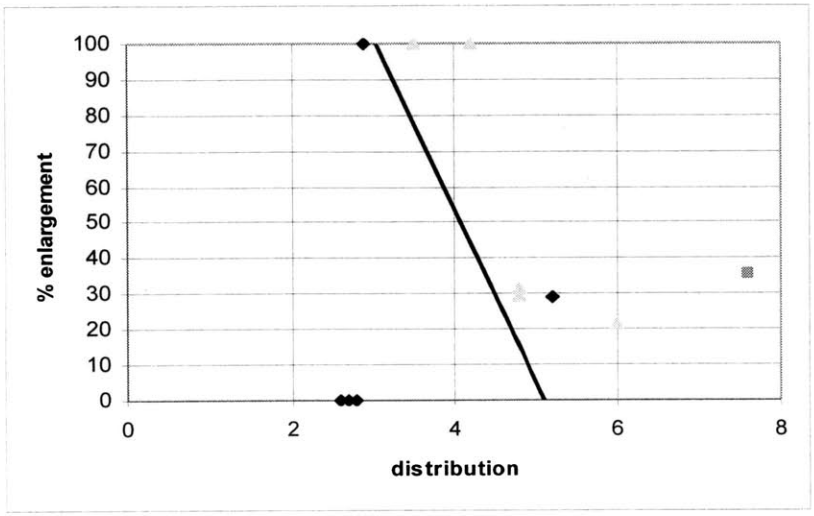

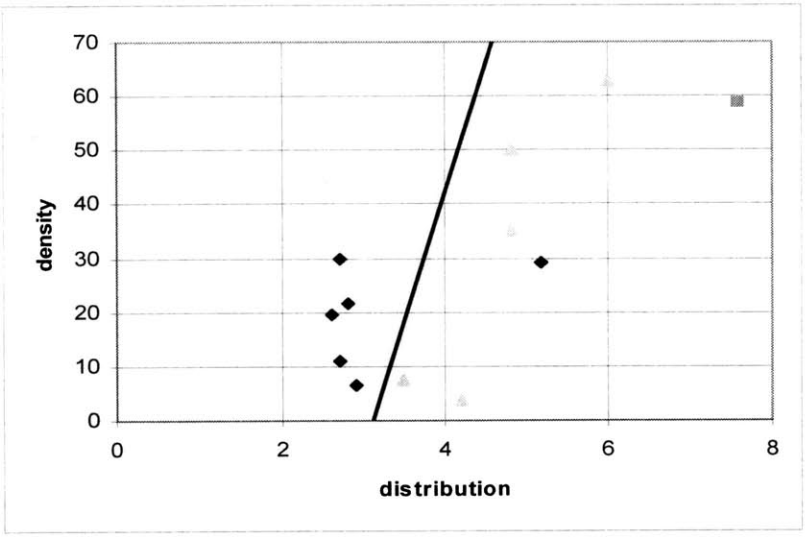

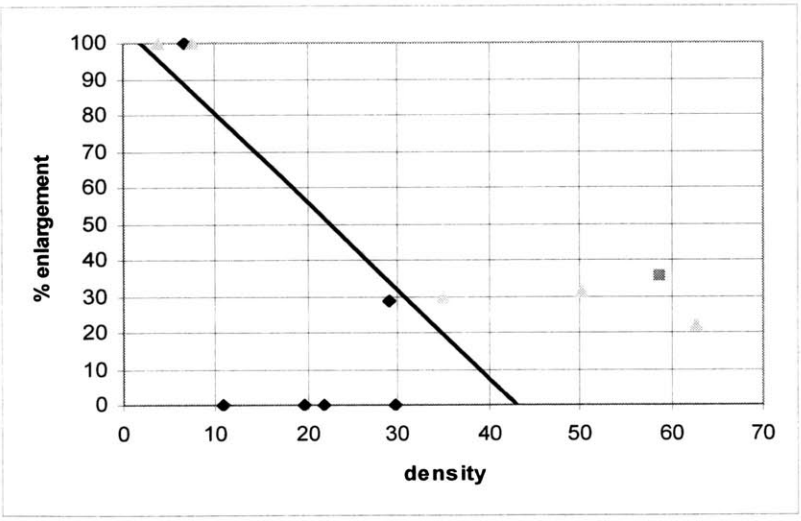

Figure 5.19: again, black diamonds for non-dysplastic, dark gray squares for low grade, and light gray triangles for high grade. Each graph has different axes, but all three differentiate between non-dysplastic and dysplastic clearly.

Table 5.1

	Non-dysplastic vs. dysplastic		High grade vs. low grade & non	
	Sensitivity	Specificity	Sensitivity	Specificity
DRS	64%	100%	75%	100%
IFS	91%	93%	100%	78%
LSS	100%	83%	100%	71%
TMS	91%	100%	91%	84%

While some of the individual results are somewhat low, particularly the diffuse reflectance sensitivity, the combination of the three techniques again shows a dramatic improvement over any one of the three techniques used alone, and its results are very reasonable. For this analysis, spectra that did not return LSS were counted as dysplastic, and IFS diagnosis was taken using a simple majority of the three fluorophore charts. It may be said that sensitivity is the more important statistic, as any false positives can be ruled out by the ensuing biopsy, but false negatives will result in a skipped biopsy and therefore an undetected dysplasia site. With that in mind, light scattering alone seems to have the best sensitivity, but alone, LSS has the drawback of being unable to analyze every data point, and thus becomes more of a corroborating technique to the other two.

Prospective analysis and verification

The remaining data was analyzed using the methods and thresholds developed above, and diagnoses were assigned to each site according to the thresholds, without prior knowledge of their pathological diagnoses. A portion of the data sites had to be rejected because the data was unusable due to several factors. Some of the data had extremely low intensity, making the signal to noise ratio too low for the data to be reliable. Other sites had nothing wrong with the data measurements, but the calibration measurements of the spectralon and rhodamine were taken incorrectly. After all the filtering of unusable

data, 396 points remained. These spectroscopic diagnoses were then compared with the diagnoses of the biopsies. The results as a whole were not quite as expected.

As detailed, the diagnostic thresholds were determined through rigorous analysis and after many modifications to yield the best results with the calibration set. And yet, when applied to the prospective set, the results were as described following.

Diffuse reflectance analysis

Figure 5.20 shows the diffuse reflectance results, plotting again the intensity of μ_s' at 600 nm with the hemoglobin absorption.

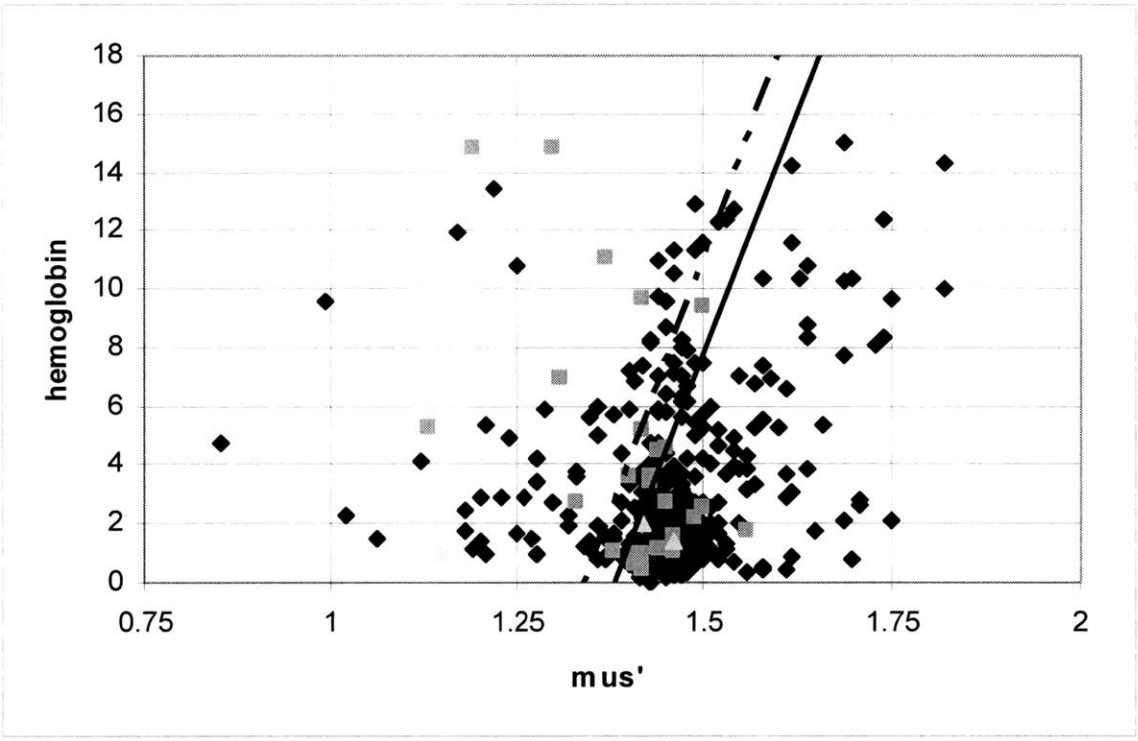

Figure 5.20: black diamonds non-dysplastic, dark gray low grade, light gray high grade. Solid line dysplasia, dashed line high grade divisions.

While the specificity is reasonable, the sensitivity is not as much. There are several possible reasons why these results came out as they did. While the idea of this

prospective set is that it would be large enough to make the general trends very clear, there are only three high grade dysplastic data sites. It is therefore impossible to assume that these three sites are representative of high grade dysplastic sites in general, and on the contrary, imply they do not fit the characteristics, as the eight high grade sites analyzed previously would provide a more representative sample. This also explains why the specificity is good while the sensitivity is not. Because there are so many non-dysplastic sites, the general trend is revealed, supporting the diagnostic thresholds developed, while the lack of dysplastic data results in an inconclusive outcome.

Another insight can be found in the segregating of the set into the two summers in which the data was taken. Looking at only the data taken in the summer of 2000, the same μ_s' plot looks instead like the following, shown in figure 5.21a. The remaining data, from the summer of 2001 is shown in figure 5.21b.

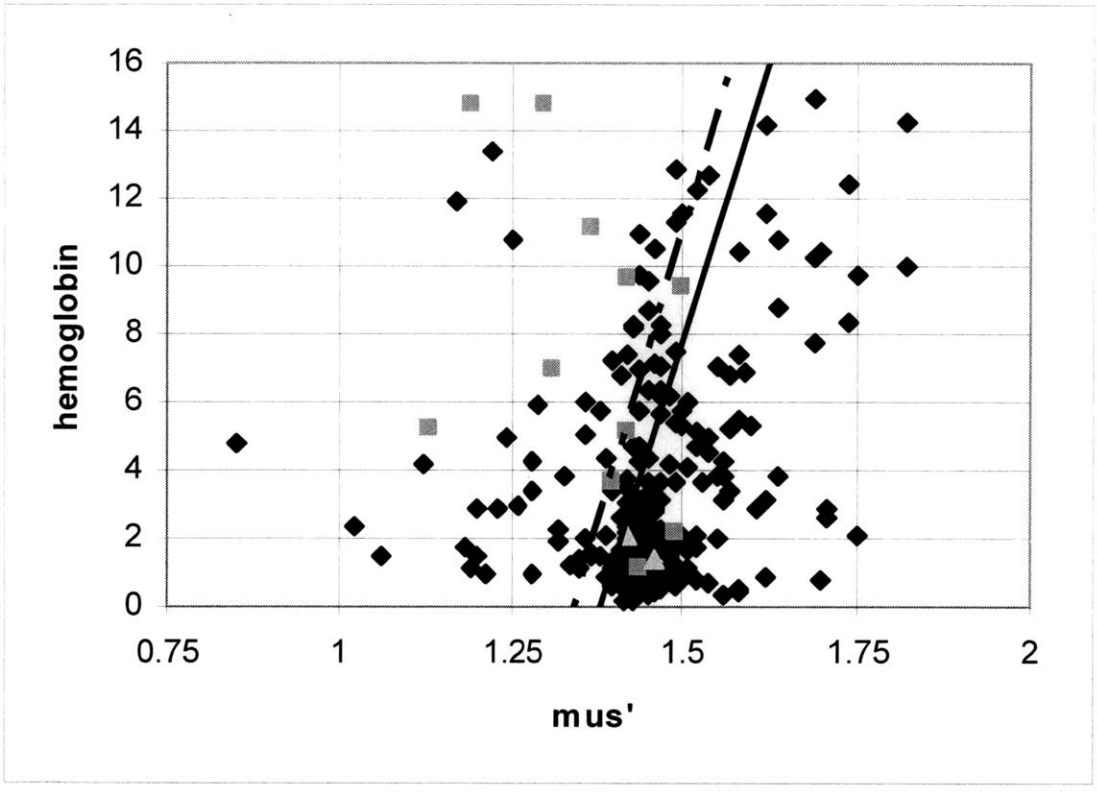

Figure 5.21a: mus' and hemoglobin plot from 2000 summer data set

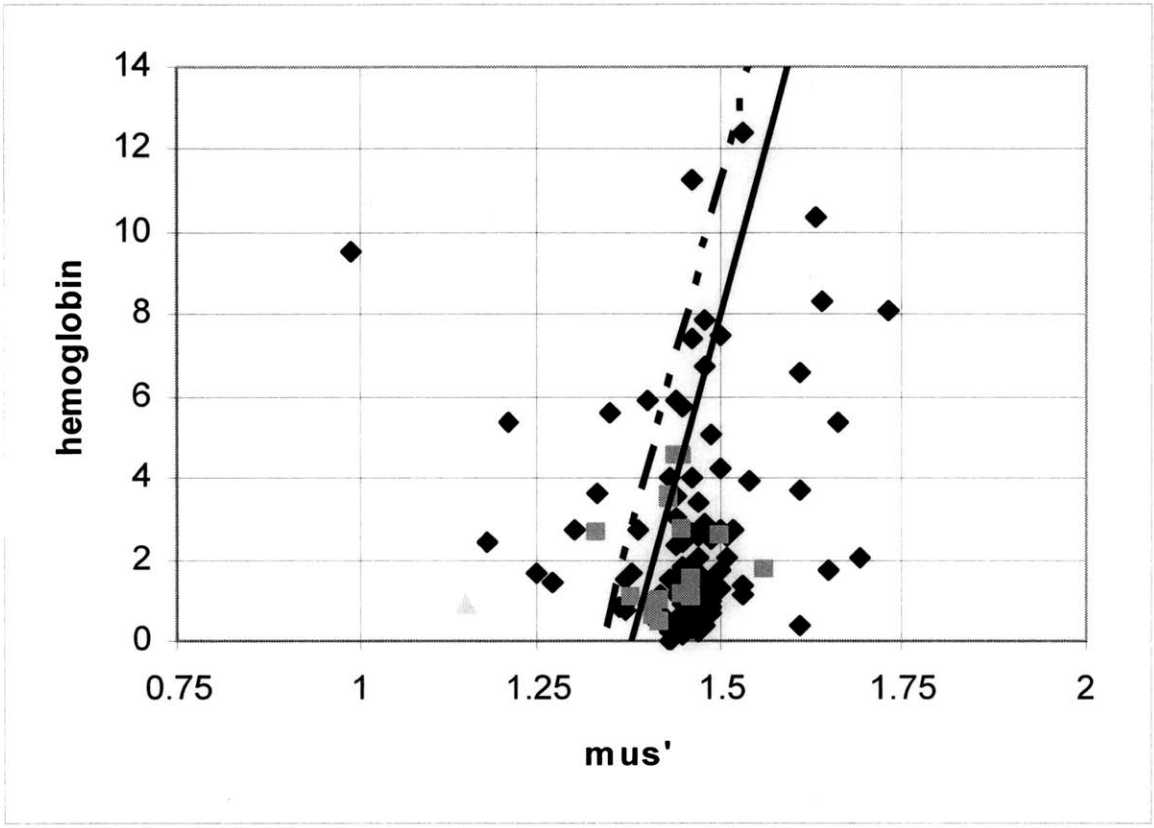

Figure 5.21b: mus' and hemoglobin plot from 2001 summer data set

While the calibration set was a mixture of data points from both years, the majority of the dysplastic data came from the former summer. The consistent discrepancy found between the two sets suggests there was some unexpected change between the two data gathering sessions. The fact that the two plots by themselves exhibit similar trends in the low grade dysplastic sites with only some scaling factor separating them supports this idea. The intrinsic fluorescence analysis results also support these explanations.

Intrinsic fluorescence analysis

The following pages contain plots for all data with each of the decompositions into the four fluorophores: collagen, NADH, porphyrin and tryptophan.

Figure 5.22 (continued on next two pages): intrinsic fluorescence decompositions

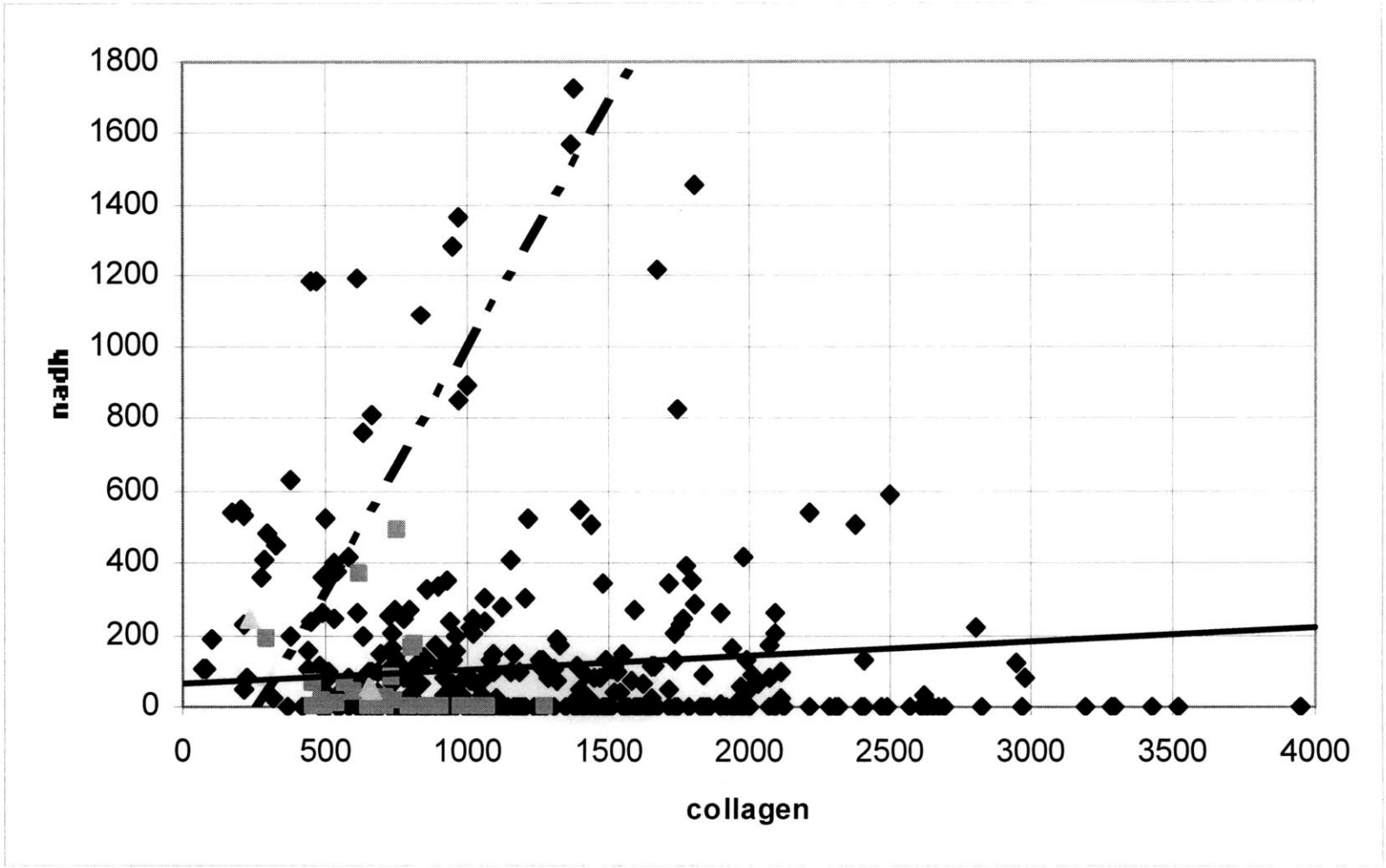

Figure 5.22: intrinsic fluorescence decompositions

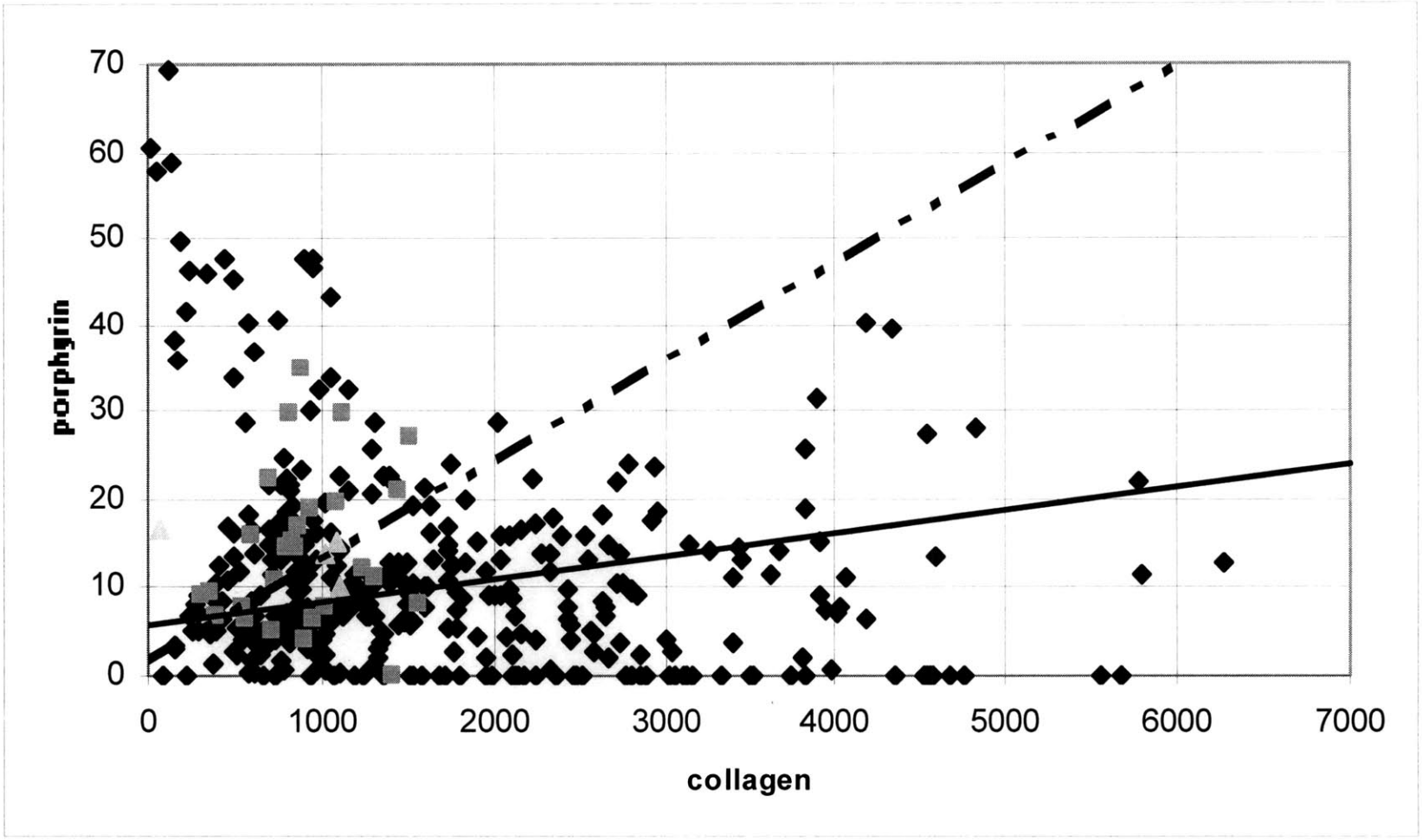

Figure 5.22: intrinsic fluorescence decompositions

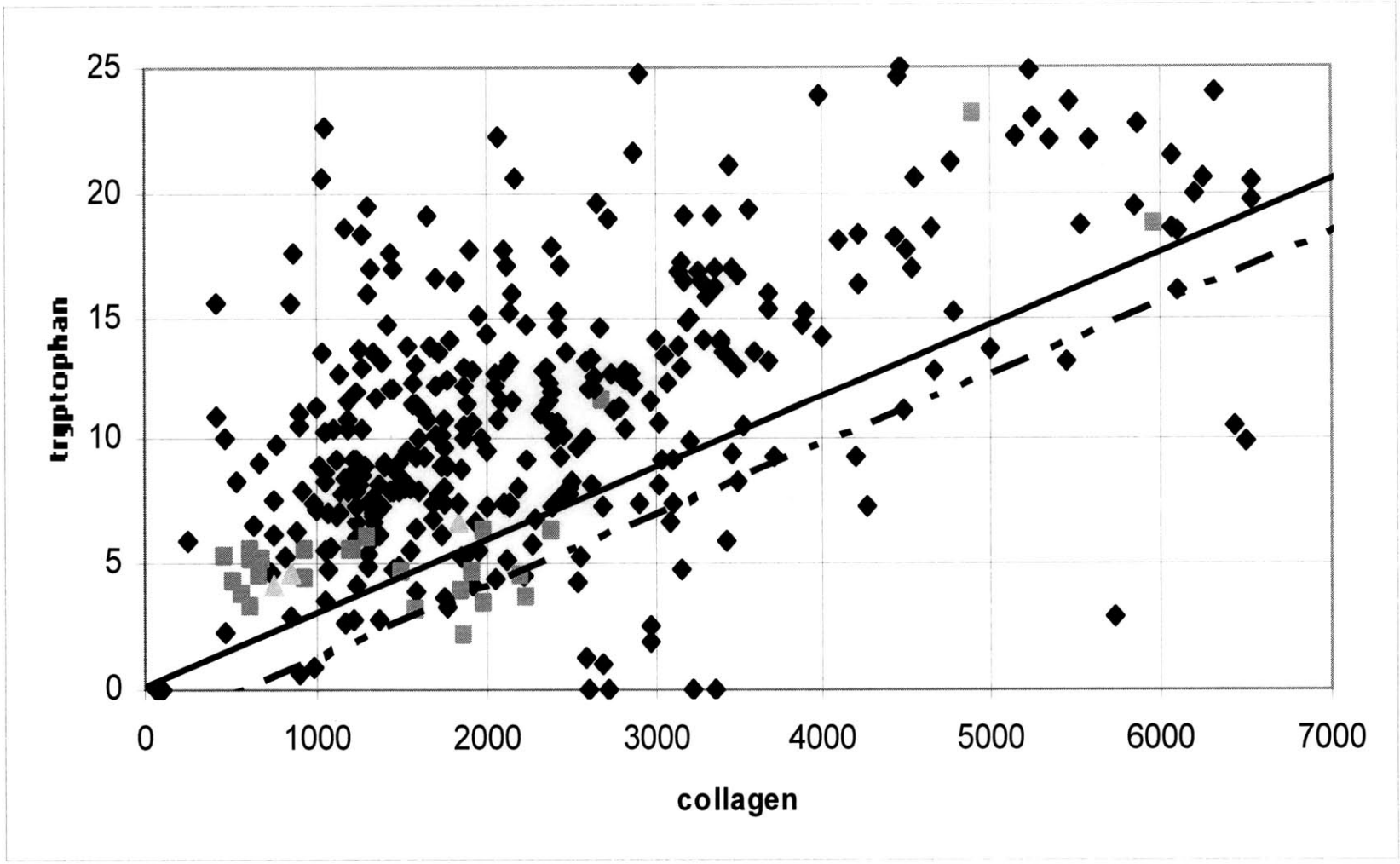

Figure 5.22 (continued from previous two pages)**:** intrinsic fluorescence decompositions

Figure 5.23: dysplasia division surface above, high grade surface below. Slope is different only because the axes have changed for a better angle. Non-dysplastic in blue diamonds, low grade green squares, and high grade red triangles.

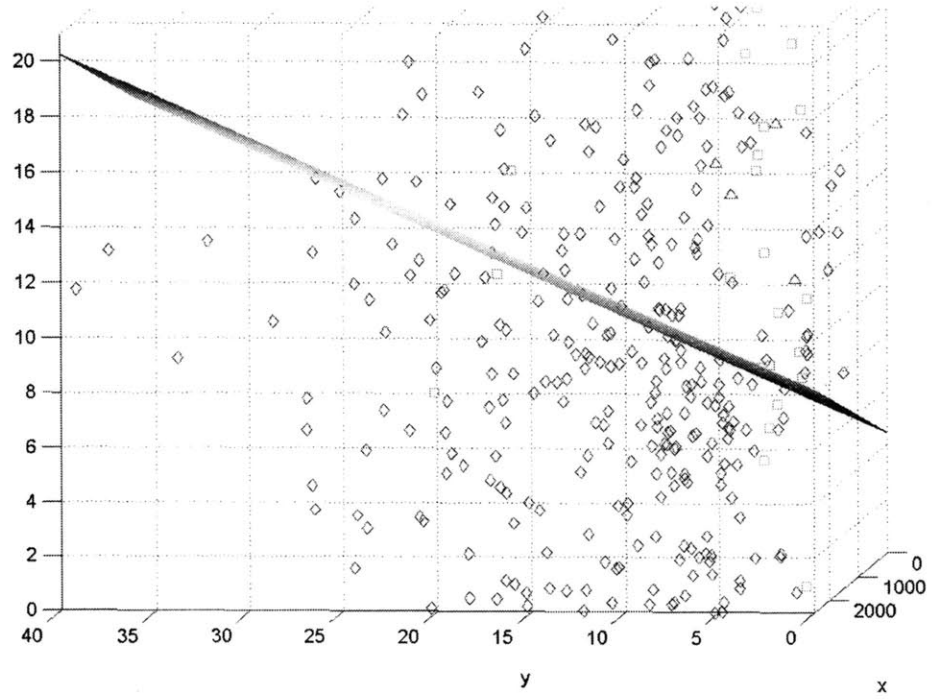

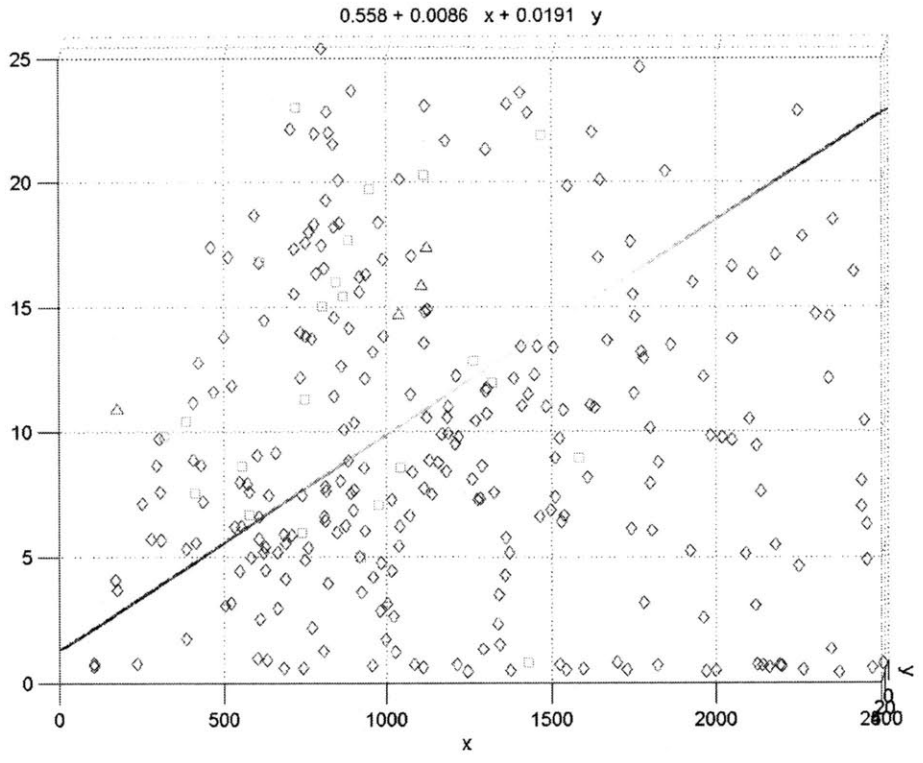

It may be somewhat difficult to identify the few dysplastic points among the numerous non-dysplastic, but what can be drawn is that the trend found with the diffuse reflectance is the same. Looking especially at the NADH and tryptophan decompositions, the specificity is again quite good. The high grade results are again too few to be reliable, and the low grade results are again divided into two groups, those taken from two years ago which fit the trends and give correct diagnoses, and those from last year which do not fit the diagnoses. Particularly in the tryptophan decomposition (figure 5.22c), two distinct groupings can be seen. Figure 5.24 shows the collagen and porphyrin concentrations for the 2000 data set.

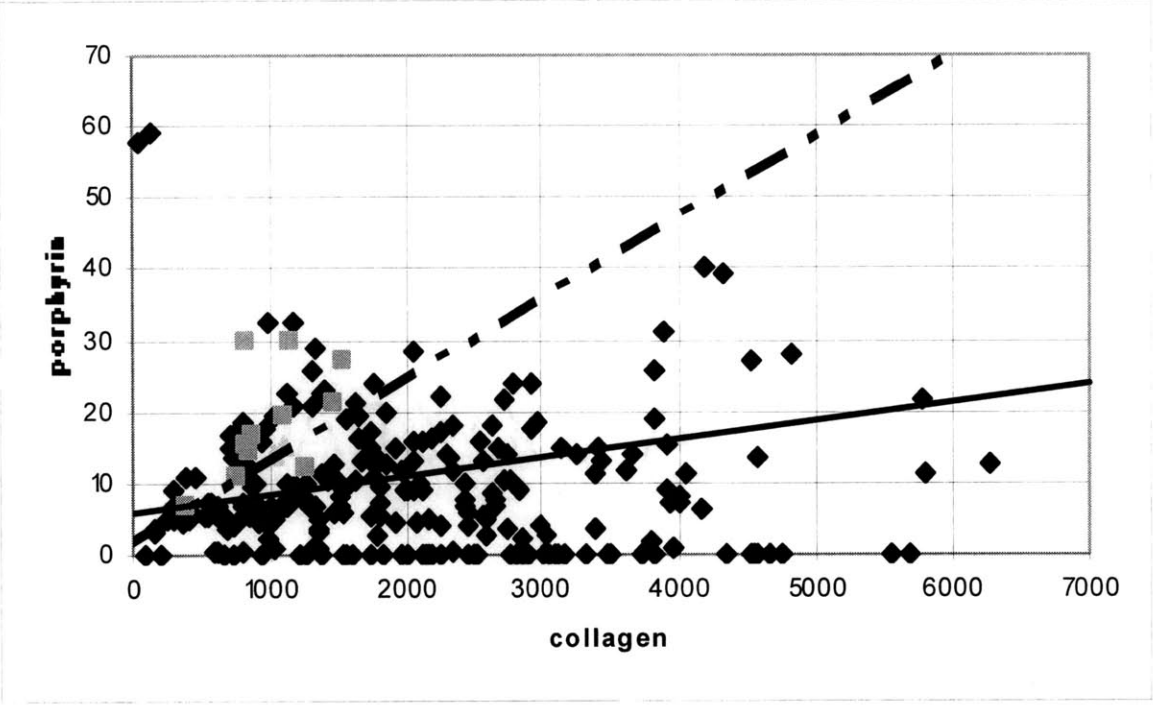

Figure 5.24: porphyrin and collagen decomposition for 2000 data set

The difference is clear, with this set having 100% sensitivity for dysplastic tissue from non-dysplastic. While this may be a fortunate case, as the high grade dysplastic data is no more reliable for this plot than with any of the previous, the argument for some unexpected change in the measuring apparatus or calibration between the two years is strong.

Light scattering analysis

The light scattering analysis is also in support of this theory, but in a slightly different way. The three result plots are shown in figure 5.25.

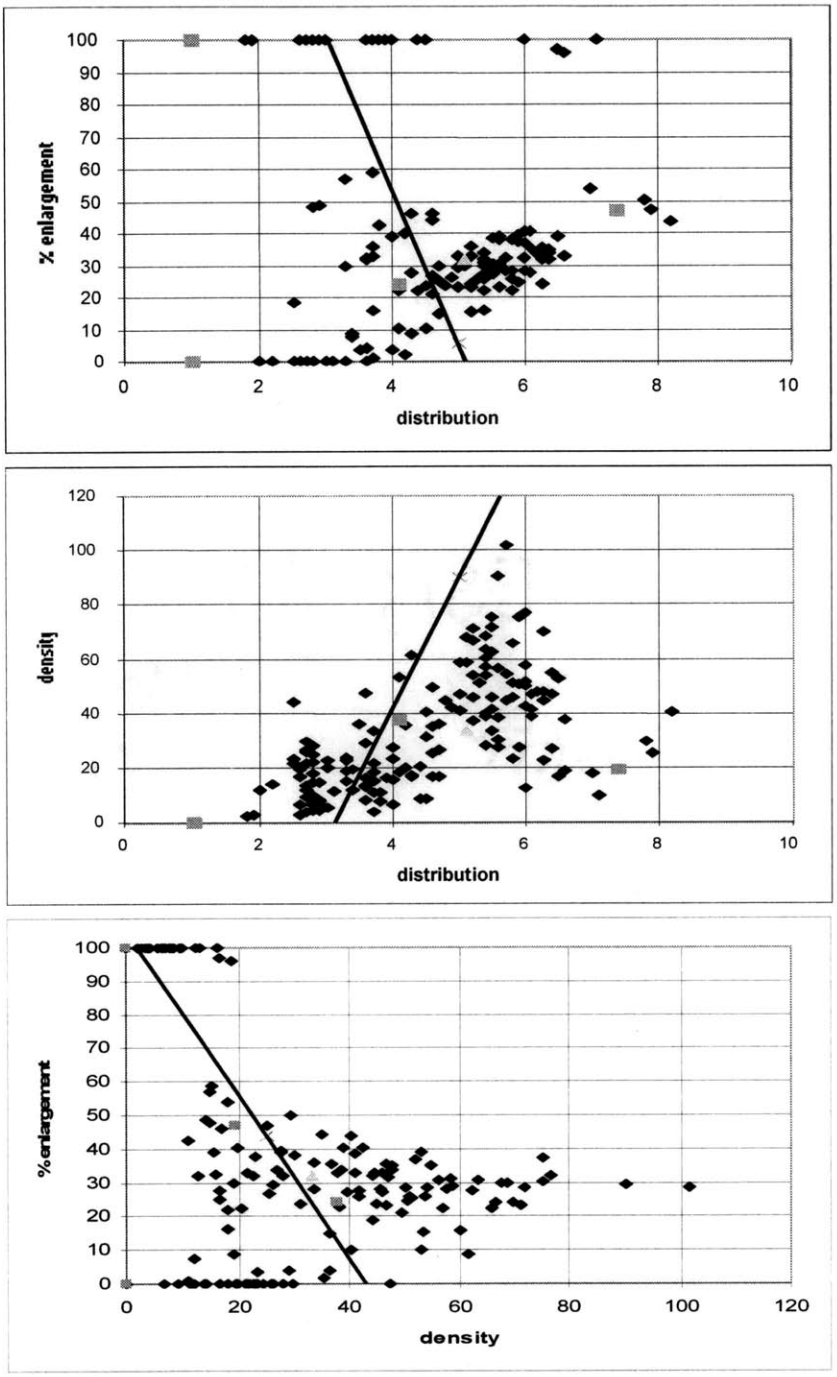

Figure 5.25: prospective LSS analysis. Black diamonds non-dysplastic, dark gray squares low grade, light gray squares high grade.

What is immediately evident is that very few of the dysplastic sites returned a light scattering spectrum. Only 45% of the sites were able to pass all the checkpoints. What is interesting is that the data that has been fitting the diagnoses gave a 55% yield rate for points that returned an analysis, better than that of the original calibration set, compared to only 25% for the later year's data set. In many of the cases, even though the model reflectance fits were better than those from the 2000 set, they failed to pass the checkpoints.

Tri-modal analysis

Given this unfortunate discovery and the small amount of dysplastic data, a tri-modal analysis would be inconclusive at best. Even to run an analysis only on the older data set would not provide much useful information, as the two high-grade dysplastic tissue data seem to be outliers. With that in mind, the tri-modal figures can be seen in table 5.2.

Table 5.2

	Non-dysplastic vs. dysplastic		High grade vs. low grade & non	
	Sensitivity	Specificity	Sensitivity	Specificity
DRS	37%	81%	33%	89%
IFS	78%	88%	33%	91%
LSS	40%	64%	100%	64%
TMS	87%	82%	33%	91%

6
Conclusion

The main goal of this study was to assess in a prospective manner the value of tri-modal spectroscopy as a real-time guide to biopsy for the detection of dysplasia in Barrett's esophagus. Specifically, diagnostic potential of three spectroscopic techniques, diffuse reflectance, intrinsic fluorescence, and light scattering, were assessed individually and in combination. Diffuse reflectance gave information about the scattering and absorption properties of the tissue, revealing changes in the prominence of collagen and hemoglobin as the tissue advances in dysplastic stages. Intrinsic fluorescence showed the changes in fluorophore concentrations, namely collagen, NADH, and porphyrins to distinguish between the tissue states. And light scattering provided information on the cell nuclei, their enlargement and crowding as the nuclei underwent the changes found typically in dysplastic tissue.

Using methods developed to model the light's interactions with the tissue, quantitative information was extracted, which is not only diagnostically useful, but also provides insights into the development of dysplasia. With diffuse reflectance, the

decrease in scattering and increase in absorption are quantitatively evident and are useful diagnostic parameters. In intrinsic fluorescence, it would seem that the concentration of porphyrins increases in the tissue before there is an increase in NADH concentration, allowing for a distinction of dysplastic grades. Tryptophan also shows an increase in concentration, and as shown its potential to be a contribution in the diagnostic process. Light scattering spectroscopy analysis revealed the diagnostic value of the modeled nuclear crowding and enlargement and also the new parameter for the distribution of nuclear sizes.

The algorithms developed and results found in the preliminary study have been corroborated and modified to work with the new generation FastEEM instrument. The diagnostic algorithms have been further improved to include information from porphyrin. Fluorescence component spectra for both porphyrin and tryptophan were experimentally extracted and used to examine the interaction of these biochemicals in the development of dysplasia. The real time aspect of the instrument was also examined and improved. All these things contributed to making a diagnostic tool that can be used in real time to aid physicians in better detecting dysplasia.

The one encountered misfortune is the unexplained systematic shift in the data from between the two times of measurement. As long as there is no such change in the future, a recalibration of the diagnostic thresholds to fit the current data would provide an accurate and valuable tool. With the prospective data set now also available to be used for further calibration, the modifications should become more accurate and sensitive as more data is used.

Future work

There are still several ways in which this instrument can be further improved. The first is evident, the determining of what it is that caused the change in data between the two years. Such changes, obviously, must be guarded against, as a recalibration for every set of data taken is impractical and unfeasible. Once this is discovered, more dysplastic data should be taken to finalize a recalibration. Several of the excitation

wavelengths are still not currently used in diagnosis. These wavelengths can be studied and examined in greater depth to determine if they are diagnostically useful. In particular, some of the fluorophores known to be present in the esophagus, such as flavin adenine dinucleotide, can be examined to see if they display some pattern of behavior with the development of dysplasia. If they are determined to be not useful, these wavelengths can be removed from the dye wheel and from the program to simplify and expedite the entire process. Replacing of the dye wheel itself may be another direction into which can be looked, as other system configurations that are more cost effective and easier to maintain may be found and more appropriate for a commercial clinical setting. For example, a third generation instrument could consist of only two to three excitation wavelengths, which provide the most diagnostically useful information. Furthermore, the software code still has room for optimizations in speed to further improve the real time feedback of the system.

As for expanding into new directions, there is no need to limit the use of this system for dysplasia in Barrett's esophagus. The principles behind this tool can be readily converted to be used in the detection of other forms of precancerous conditions in other parts of the body. Much of the spectroscopic experimentation has already been done, as referenced in the background, and so the initial steps to develop diagnostic algorithms have already been taken. Each tissue does, however, have its own characteristic biochemistry and morphology, and while models and diagnostic algorithms need to be modified to account for these differences, the potential is undeniable.

iii
Bibliography

Arendt JT. "Detection of early cancerous changes and cancer in bladder tissue by autofluorescence and reflectance." V-1, thesis, School of Ohio State University, 1999.

Bigio IJ and Mourant JR. "Ultraviolet and visible spectroscopies for tissue diagnostics: fluorescence spectroscopy and elastic-scattering spectroscopy." *Phys Med Biol.* 1997, 42:803-14.

Cameron AJ, Lomboy CT. "Barrett's Esophagus: Age, prevalence, and extent of columnar epithelium." *Gastroenterology.* 1992, 103(4):1241-5.

Cotran, RS, Robbins, SL, Kumar, V. *Robbins Pathological Basis of Disease.* Philadelphia: 1994.

Farrell TJ, Patterson MS, Wilson B. "A diffusion theory model of spatially resolved, steady-state diffuse reflectance for the noninvasive determination of tissue optical properties in vivo." *Med. Phys.* 1992, 19 (4), 879-888.

Fisher L, VanBelle G. *Biostatistics: a Methodology for the Health Sciences.* New York: Wiley, 1993.

Fred Hutchinson Cancer Research Center. "Barrett's Esophagus in Plain English." http://www.fhcrc.org/phs/barretts/plain.htm. 1998.

Georgakoudi, I, Jacobson, BC, Van Dam, J, Backman, V, Wallace, MB, Muller, MG, Zhang, Q, Badizadegan, K, Sun, D, Thomas, GA, Perelman, LT, Feld, MS. "Fluorescence, Reflectance, and Light-Scattering Spectroscopy for Evaluating Dysplasia in Patients with Barrett's Esophagus." *Gastroenterology.* 2001, 120:1620-29.

Gopal, Depak V. "Another look at Barrett's Esophagus: Current thinking on screening and surveillance strategies." *Postgraduate Medicine* 2001, 110(3):57-68.

Lovat, LB, Pickard, D, Novelli, M, Ripley, PM, Francis, H, Bigio, IJ, Bown, SG, "A novel optical biopsy technique using elastic scattering spectroscopy for dysplasia and cancer in Barrett's esophagus." *Gastroint. Endoscopy.* 2000, 51:4919.

National Institutes of Health. "Barrett's Esophagus." Publication No. 99-4546. http://www.niddk.nih.gov/health/digest/summary/barretts/barretts.htm. May, 1999.

Newton, RG. *Scattering Theory of Waves and Particles.* McGraw-Hill, New York: 1969.

Pagano M, Gauvreau K. *Principles of Biostatistics.* Belmot, CA: Duxbury Press, 1993.

Prahl, Scott. "Optical Absorption of Hemoglobin." Oregon Medical Laser Center. http://omlc.ogi.edu/spectra/hemoglobin/summary.gif. December 1999.

Reid, BJ, Haggitt, RC, Rubin, CE. "Observer Variation in the Diagnosis of Dysplasia in Barrett's Esophagus." *Human Pathology*. 1988, 19:166-178.

Richards-Kortum R, Rava RP, Fitzmaurice M, Kramer JR, Feld MS. "476 nm excited laser-induced fluorescence spectroscopy of human coronary arteries: applications in cardiology." *Am Heart J.* 1991, 122:1141-50.

Riddell, R, Goldman, H, Ransohoff, D, Appelman, HD, Fenoglio, CM, Haggitt, RC, Ahren, C, Correa, P, Hamilton, SR, Morson, BC, Sommers, SC, Yardley, JH. "Dysplasia in Inflammatory Bowel-Disease, Standardized classification with provisional clinical applications." *Human Pathology*. 1983, 14:931-968.

Schantz SP, Kolli V, Savage HE, Yu G, Shah JP, Harris DE, Katz A, Alfano RR, Huvos AG. "In vivo native cellular fluorescence and histological characteristics of head and neck cancer." *Clin Cancer Res.* 1998, 4:1177-82.

Schnell, T, Sontag, S, Wanner, J, et al. abstract. *Gastroenterology.* 1985, 88:1576.

Schumacher M, Hollander N, Sauerbrei W. "Resampling and cross-validation techniques: a tool to reduce bias caused by model building?" *Stat Med.* 1997, 16:2813-2827.

Van Houwelingen JC, Le Cessie S. "Predictive value of statistical models." *Stat Med.* 1990, 9:1303-1325.

Vo-Dinh T, Panjehpour M, Overholt BF. "Laser-induced fluorescence for esophageal cancer and dysplasia diagnosis." *Ann NY Acad Sci.* 1998, 9:116-22.

Winters, C Jr., Spurling, TJ, Chobanian, SJ, et al. "Barrett's Esophagus: A prevalent, occult complication of gastroesophageal reflux disease." *Gastroenterology*. 1987, 92:118-24.

Zhang, Q, Muller, MG, Wu, J, Feld, MS. "Turbidity-free fluorescence spectroscopy of biological tissue." *Optics Letters*. 2000, 25:1451-1453.

Zonios, George, Perelman, LT, Backman, V, Manoharan, R, Fitzmaurice, M, Van Dam, J, Feld, MS. "Diffuse reflectance spectroscopy of human adenomatous colon polyps *in vivo*." *Applied Optics*. 1999, 38(31):6628-37.